FACULTY
OF MATHEMATICS
AND PHYSICS
Charles University

MASTER THESIS

Zdeněk Krtouš

Tailoring of structure of plasma polymers

Department of Macromolecular Physics

Supervisor of the master thesis: Mgr. Jaroslav Kousal, Ph.D.

Study programme: Master

Specialization: Physics of Condensed Matter and Systems

Prague 2020

Declaration

I declare that I carried out this master thesis independently, and only with the cited sources, literature and other professional sources.

I understand that my work relates to the rights and obligations under the Act No. 121/2000 Coll., the Copyright Act, as amended, in particular the fact that the Charles University has the right to conclude a license agreement on the use of this work as a school work pursuant to Section 60 paragraph 1 of the Copyright Act.

In Jablonec nad Nisou, 6 January 2020

Zdeněk Krtouš

Acknowledgments

Research for and elaboration of this Master thesis was funded by the Czech Science Foundation, project registration no. 17-10813S “Novel Plasma Polymers with Tunable Stability and Permeability”. I am grateful to Danill Nikitin, Mikhajlo Vaydulich and Pavel Pleskunov for participation on XPS measurements and Jan Hanuš for help with XPS interpretation. I thank Lenka Hanyková for measurements and quantifications of NMR spectra. I am grateful to Ivan Krakovsky for measurements and analysis of results from GPC
technique. Pavel Solař helped me with development of deposition control software. I am grateful to Zuzana Kolářová Rašková, Jana Sedlaříková and Liliana Kučerová from Tomas
Bata University in Zlín for provision of the precursor and measurement and analysis of stability in water properties. Finally, I thank to Jaroslav Kousal for his help with analysis of
ellipsometric data and his extremely helpful supervision of this Master thesis.

Information

Title: Tailoring of structure of plasma polymers

Author: Zdeněk Krtouš

Department: Department of Macromolecular Physics

Supervisor of the master thesis: Mgr. Jaroslav Kousal, Ph.D., Department of Macromolecular Physics, Faculty of Mathematics and Physics, Charles University

Abstract: The thesis was targeted on the preparation of thin film plasma polymers with Plasma assisted vapour thermal deposition technique. As a characterised precursor was chosen the poly lactic acid because of its interesting biodegradable properties. The set of samples prepared with varying plasma power was obtained. It was found that the PLA structure is still preserved after repolymerisation, moreover, new carbon rich compound was formed. The strong changes of behaviour of samples in water were observed around plasma power of 30 W. The sample prepared in weaker plasma had properties of hydrogel. The samples prepared above 30 W of plasma power were solid and did not dissolve in water.

Keywords: PAVTD, PLA, plasma polymer

Název práce: Řízení struktury plazmových polymerů

Autor: Zdeněk Krtouš

Katedra: Katedra makromolekulární fyziky

Vedoucí diplomové práce: Mgr. Jaroslav Kousal, Ph.D., Katedra makromolekulární fyziky, Matemeticko-fyzikální fakulta, Univerzita Karlova

Abstrakt: Diplomová práce cílila na přípravu tenkých vrstev plasmových polymerů technikou plazmově asistované termální depozice. Jako charakterizovaný prekurzor byla vybrána kyselina polymléčná pro své zajímavé biodegradabilní vlastnosti. Vzorky byly připraveny za různých výkonů plazmatu. Bylo zjištěno, že struktura kyseliny polymléčné je po repolymerizaci zachována a nadto vzniká složka bohatá na uhlík. Vzorky připravené za různých výkonů plazmatu vykazovali velice rozdílné vlastnosti po ponoření do vody. Byly naměřeny velké změny vlastností připravených vrstev po ponoření do vody. Vrstvy připravené při výkonech menších než 30 W vykazovali charakter hydrogelu. Vzorky připravené za vyšších výkonů byly kompaktní a ve vodě se nerozpustily

Klíčová slova: PAVTD, PLA, plasmový polymer

Contents

Introduction

Nowadays we live in a plastics age. The plastic, also known as polymeric or macromolecular materials are everywhere around us. These materials are used as building materials, in medicine, electronics, package materials and in many other applications. Typically, these materials are required in large amounts and are used in their bulk form. Materials like 1D fibres or 2D thin films are required for some applications. For example, protecting and barrier layers, optically active materials, coatings with a large surface for catalysis and others. These applications are mostly accomplished using wet chemistry methods, like spin coating, Langmuir-Blodgett method and other techniques. [1,2] This thesis is mainly focused on preparation and characterisation of layers with controlled composition and stability in water that can be potentially used as biodegradable barrier coatings. One of the most widely used biodegradable polymers is polylactic acid (PLA). Presence of network-like structure in such polymers influence their degradability and stability, but it is difficult to obtain high density of crosslinks in these materials through classical chemistry methods.

Even though these wet chemistry methods are wide-spread and industrially important, they are accompanied by negative aspects. Firstly, they may be environmentally unfriendly as toxic chemistry compounds may be used during these processes. Secondly, those classical chemistry techniques work close to thermodynamic equilibrium limiting the possible reaction pathways. Some of these negative aspects of wet chemistry can be overcome by synthesis of materials in plasma. Using nonequilibrium plasma as an active medium can hugely modify the resulting products of deposition. The thermodynamical equilibrium of synthesis can be shifted to forming nanoparticles, or composites of non-mixable materials, which would not be possible to prepare in equilibrium.

The plasma assisted synthesis of thin polymeric films can be divided into two groups: The atmospheric pressure deposition and deposition at the lowered pressure. Several different techniques of deposition may be used in both groups, such as physical vapor deposition (PVD), chemical vapor deposition (CVD), magnetron sputtering and other vacuum techniques and plasma jet, dielectric barrier discharge (DBD) and other atmospheric techniques. The resulting polymer-like layers prepared in plasma have different properties from bulk polymers and are called “plasma polymers”.

Aims of this Thesis

Focus on preparation and characterization of plasma polymers with high retention of classical chemical structure. The main goal consists of several subtasks:

- Development and optimization of deposition of plasma assisted vapour thermal deposition setup.
- Deposition of thin films in this setup under a range of conditions.
- Analysis of chemical composition of these films.
- Characterization of films stability in water

1 Theoretical Part

1.1 Plasma

Plasma is a medium a collective behaviour due to presence of free charge carriers, typically in a form of ionized gas consisting of a electrically quasi neutral mixture of electrons, ions, neutral atoms, radicals and photons. Plasma is characterised by ionization degree.

$$\alpha = \frac{N_i}{N_i + N_n}, \quad 1)$$

where N_i is the number of Ions and N_n is the number of neutral atoms in plasma. Based on the relative temperatures of the plasma species, plasma can be classified as thermal (equilibrium) or non-thermal (non-equilibrium) plasma [3,4]. A thermal plasma is a plasma in thermodynamic equilibrium when electrons have the same temperature as heavy species ($T_{electrons} = T_{ions} = T_{gas}$).However, in most electric discharge plasmas this is not true. ($T_{electrons} \gg T_{ions} > T_{gas}$).

Plasma is defined by its characteristic length – the Debye length. The Debye length quantifies the electrical screening of charge introduced into plasma by surrounding charged and can be calculated as follows:

$$\lambda_D = \sqrt{\frac{\epsilon_0 T}{e n_e}}, \quad 2)$$

where ϵ_0 is the permittivity of vacuum, T is the temperature in eV of electrons, e is charge of an electron and n_e the density of electrons. The plasma can exist only if the size of the plasma is larger than the Debye length.

Another important plasma parameter is plasma frequency. When electrons are disturbed by electromagnetic interaction the local charge imbalance occurs. Since the interaction between electrons is strong this leads to the rapid oscillation of the electron density at a frequency known as plasma frequency.

$$\omega_{pe} = \sqrt{\frac{e^2 n_e}{\epsilon_0 m_e}}, \quad 3)$$

, where m_e is the mass of the electron.

1.2 Glow Discharge

A simple example of non-equilibrium low pressure plasma is a glow discharge. Typically, we use an evacuated chamber with the pressure of working gas in the range of 0.1-10 Pa. The plasma is then ignited between two electrodes with potential difference. Volt ampere characteristic of discharge in low pressure gas is shown in figure (1).

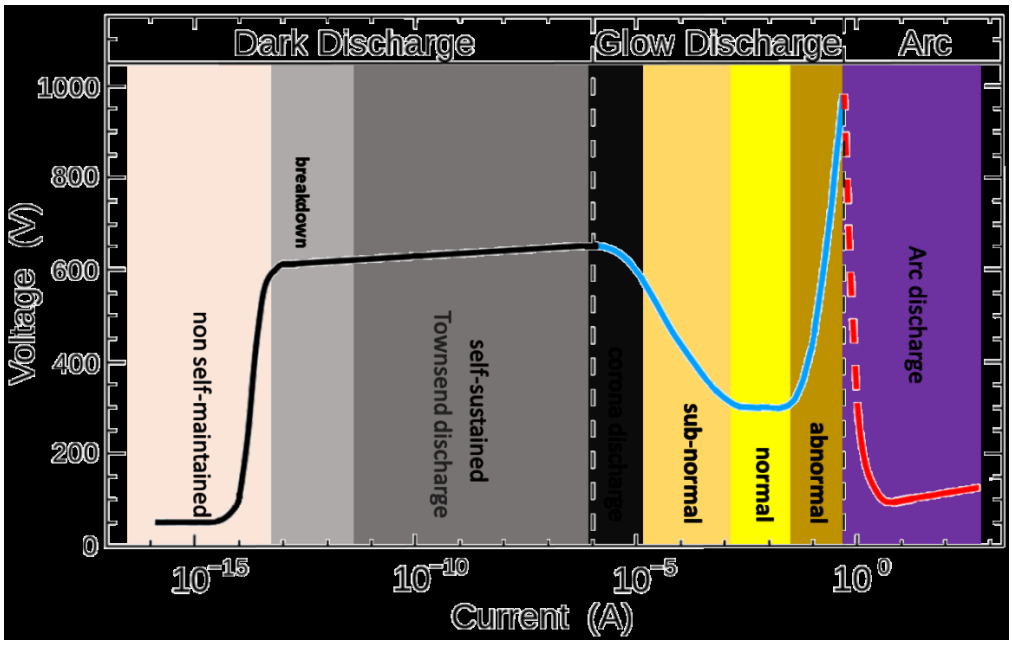

Figure 1. *Volt currect characteristic of discharge in gas. Reptinted from [5]*

The minimum voltage necessary to ignite self-sustained discharge is called breakdown voltage. The breakdown voltage depends on the product of a distance between the electrodes and pressure. The usual experimental dependence is shown in the figure (2) and is described by the following formula[6]:

$$\mathrm{V} = \frac{B(p \cdot d)}{C + \ln(p \cdot d)}, \qquad 4)$$

Where the V is breakdown voltage, p is pressure, d is distance between electrodes.

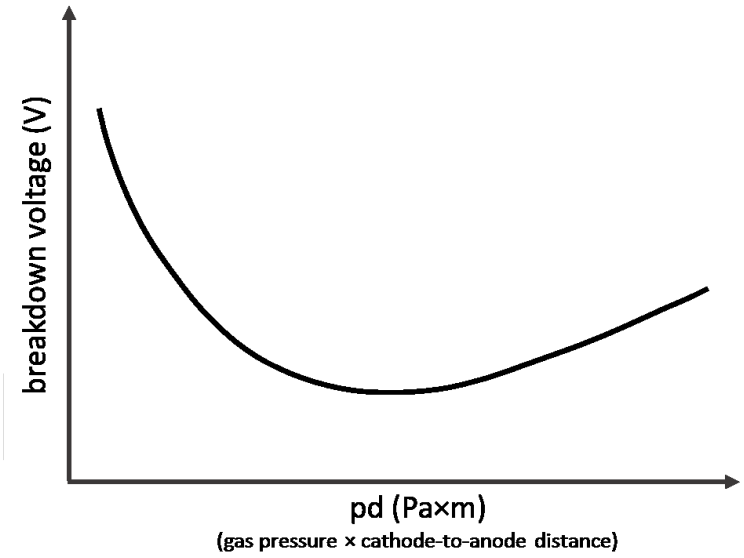

Figure 2. *Pachsen´s law*

Below the breakdown voltage the density of the electron is low and no glow can be observed.

When the voltage exceeds a breakdown value, free electrons are sufficiently accelerated (several of eV) to ionize neutral working gas and to form new free electrons. New electrons are accelerated contributing to the ionization process and forming an avalanche. As a result, self-sustained discharge is established. This type of discharge is called the Townsend discharge.

Further decrease of the external resistance leads to an increase of the current and decrease of the voltage. The subnormal glow discharge is established. When the voltage reaches steady state the discharge is called normal glow discharge. The higher the current is, the larger surface of the electrode is included in the discharge. When the whole electrode is used, the current streaming through the plasma can be increased only by increasing the voltage leading to abnormal glow discharge. Further current increase results in arc discharge, when electrons are emitted from cathode thermally.

1.3 Plasma Polymers

‘’The term plasma polymer denotes a material that is created as a result of a passage of an organic gas or vapour through the glow discharge - more generally, one should say an electric discharge in an organic gas.’’[4] The plasma or more specifically the ions, electrons, excited species and atoms forming plasma work as fragmentation agents.

Because of the randomness of all of these processes the resulting structures are typically very different from bulk polymers. The chains of plasma polymers are typically short and in addition they are randomly branched and terminated with a high degree of crosslinks. In most cases, a great number of free radicals are trapped within the network. The hypothetical structure of plasma polymer is depicted in figure (3) on the right side. On the left side at figure is shown the structure of polyethylene. [4]

a)

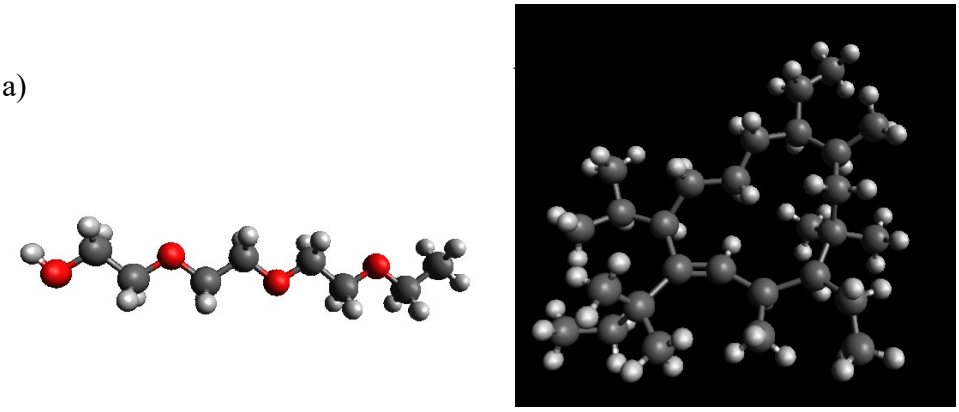

Figure 3. *a) Poly-Ethylene Glycol (PEG) structure b) Hypothetical plasma polymer structure (redrown according to [4])*

1.4 Plasma Polymer Growth Models

The simplest plasma polymerization model was described by Lam and is called free-radical plasma polymerization. This model, which describes also classical polymerization, is divided into three parts. Firstly, the molecules of precursor are initiated. Typically, the precursor is fragmented by an electron and two radicals are formed. Secondly, the precursor units are repeatedly added and whole molecule is extended. Lastly, the process is terminated by adding an end group or by merging two radical molecules together. The scheme is depicted in figure (4) [7]

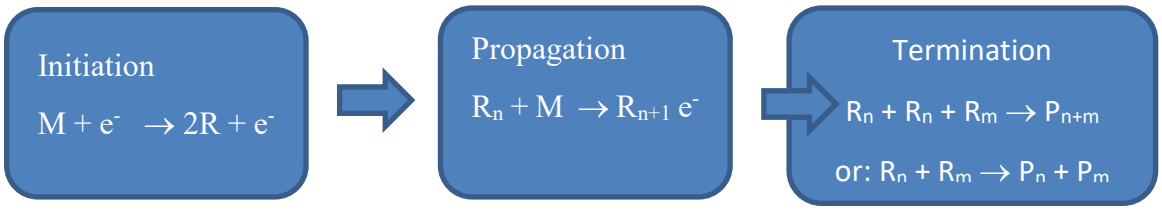

Figure 4. *Free-radical mechanism of plasma polymerization elaborated by Lam*

Yasuda introduced a new pathway in this polymerization mechanism, where multi-radical precursors are formed. This polymerization centres allow the molecule to grow in

different directions. This model is called rapid step-growth polymerization. (figure(5))

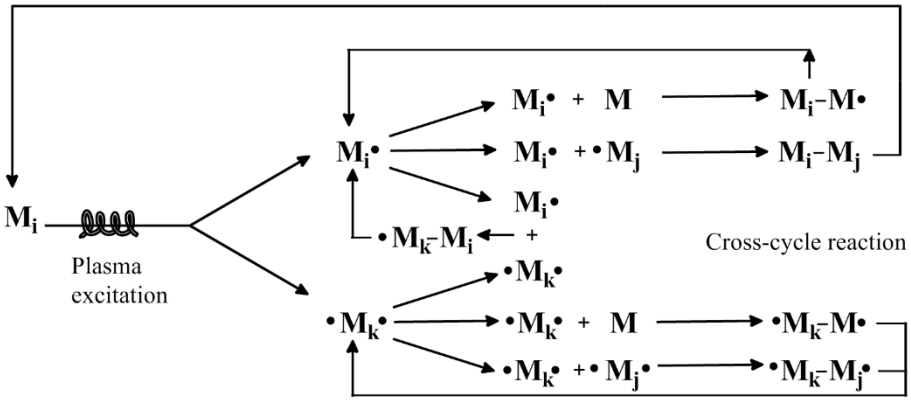

Figure 5. *rapid step-growth polymerization elaborated by Yasuda.[6]*

Another step was done by d'Agostino and described at [8] by Favia as the Activated Growth Model build up for fluorocarbon polymers. This model assumes interaction with the substrate layer, which must be activated in order to bond with growing radicals in the gas phase. The process is shown in figure (6).

1. *Fragmentation of monomer in the plasma*
   Monomer -> nCF_x
2. *2 .Ion-activation of coating(substrate)*
   I^+ (low energy) + (coating) -> $(coating)_n^*$
3. *Growth of the coating*
   CF_x <-> $CF_{x(adsorbed)}$
   $CF_{x(adsorbed)}$ + $(coating)_n^*$ -> $(coating)_{n+1}$

Figure 6. *The Activated Growth Model by d'Agostino.[4]*

, where I^+ (low energy) are low energetic Ions, $(coating)_n^*$ is activated surface.
As was shown on d'Agostino model the polymerisation processes are localised not only in gas phase in plasma, but also on the substrate. This can be also considered for a simple Lam model by considering where the initiation, propagation and termination occurs.

1.5 Yasuda Parameter

The above models describe the mechanism of plasma polymerisation. These polymerization processes are guided by deposition conditions like geometry of vacuum

chamber, duty cycle, position of sample in or outside the plasma, flow rate, power delivered in plasma and others. Yasuda came with a simple scaling law connecting flow rate and power.

$$Y = \frac{power}{flow\ rate.molar\ mass\ of\ precursor} \qquad 5)$$

While the range of validity of this scaling law is limited Yasuda parameter or its derivatives allow us to compare the degree of plasma polymerisation for different precursors, plasma powers, and flow rates [9,10] or deposition rates [30]From the energetic point of view the lighter precursor molecules can more easily polymerise and form densely crosslinked networks. This trend can be seen in figure (7), where for comparable level of polymerisation, heavier precursors have to be prepared in a higher power/flow rate ratio.

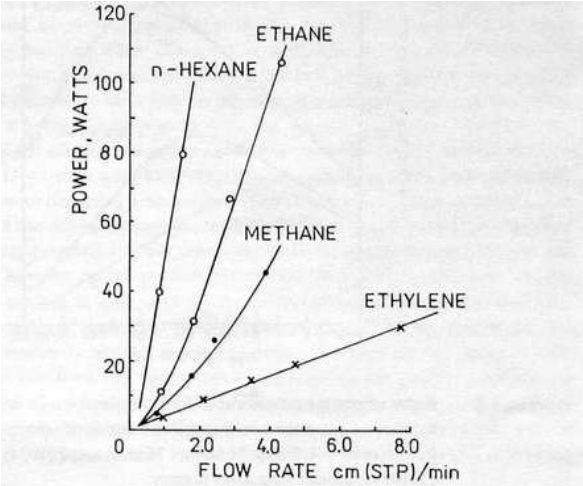

The dependence of the discharge power necessary to obtain a comparable level of glow discharge polymerization on the monomer flow rate. The necessary discharge power is greatly dependent on the molecular weights of the starting materials. Reprinted with permission from H.Yasuda and T.Hirotsu, J. Polym. Sci., Polym. Chem. Ed., 16 (1978) 743; Copyright (1978) J. Wiley & Sons, Inc.

Figure 7. *Dependence of the discharge power necessary to obtain a comparable level of polymerization*

1.6 Plasma Assisted Vapour Thermal Deposition

The plasma assisted vapour thermal deposition (PAVTD) is a deposition technique for preparation of thin films of plasma modified polymers. This technique has been studied on department of macromolecular physics at Charles university for several years. PAVDT has been employed in this lab for preparation several different types of plasma polymers. For example [11,12,13,14,15]

The PAVTD principle is similar to classical plasma enhanced chemical vapour deposition (PECVD), where the vapour of precursor is brought to plasma. In PECVD the vapour reacts with active species of plasma and it is plasma polymerized. The main difference between PAVTD and PECVD is the way, how the precursor is brought to plasma. In PECVD the precursor is transported from external source. This limits the type of the precursor, as only lower molecular compounds typically containing less than 5 to 10 carbon atoms can be used, because molecules with higher molar mass do not have enough volatility. The PAVTD overcomes this restriction. In the basic setup without plasma the precursor in solid state is placed in the heating cell – T on figure (8). The precursor is heated under the lowered pressure. With increasing temperature, the precursor becomes more volatile, is thermally fragmented and evaporated. The evaporated oligomeric fragments condense on the substrate holder-Q on figure (8). By observing the deposited polymer prepared without plasma, it was found that the typically molar mass of deposited molecules is in the range 10^{-3}mol^{-1}. Such ‘’monomer’’ with high molar mass would be difficult introduce into the plasma in a gas phase, because it would condense, before it would reach the plasma zone.

The above described setup of PAVTD without plasma corresponds to well-known physical vapour deposition (PVD). The polymeric films prepared by PAVTD without plasma technique does not have good mechanical properties as they are similar to vax. [16,17]

The situation changes when the plasma is ignited in this setup. The fragmentation and recombination of the evaporated precursor happens with higher rate than in the above described setup without plasma. The final film is formed by smaller but more densely crosslinked fragments. This crosslinking density can be modified by intensity of plasma. The plasma can be ignited in different ways. In the figure (8) is shown the RF electrode

placed below the heating cell-M. The setup with antenna type of RF electrode was tried and is described in chapter (11).

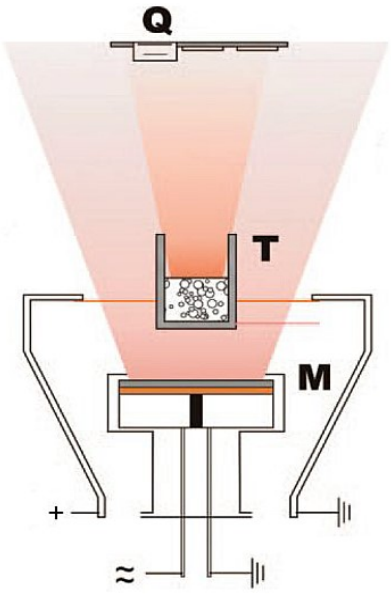

Figure 8. *Scheme of PAVTD deposition setup. T- heating cell, M – RF electrode, Q – substrate holder [14]*

2 Materials and Methods

2.1 Precursor Poly Lactic Acid

Polylactic acid (PLA) is a biodegradable polymer. Such kind of degradable polymers have important applications in the biomedical field as well as for packaging, food industry and medicine [18,19,20,21,22,23,24,25,26].

The decomposition of PLA in a water solution is based on the hydrolysis of lactic acid groups. The biodegradation is proceeded from the volume as well as surface. Polylactic acid is typically synthesized by polycondensation of lactic acid [27]. PLA (molar mass mw=10000-20000 $g.mol^{-1}$) in powder form prepared by polycondensation according to [28] was used as a source polymer for the process in this work. The typical dose of the PLA powder was 1 g per a set of depositions (3 – 5 conditions).

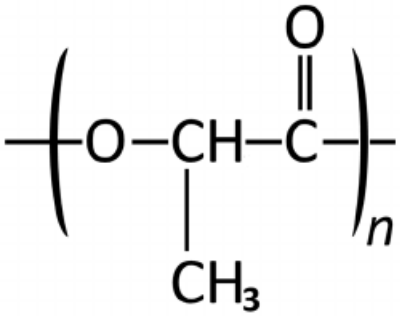

Figure 9. *PLA*

2.2 Characterisation Techniques

2.2.1 Quartz Crystal Microbalance (QCM)

Quartz Crystal Microbalance was used for measuring in-situ deposition rate. The quartz crystal with electrodes is placed in an oscillation circuit. The crystal oscillates on its normal mode, which is:

$$f = \frac{v_p}{2t}, \qquad 5)$$

where v_p is the speed of lateral elastic wave and t is the thickness of the crystal. If the mechanic properties of the deposited films are similar to the quartz crystal, then we can assume that the speed of lateral elastic wave does not change with deposited layer. Therefore, the relative thickness of the deposited film is estimated from changes of frequency during deposition. This method of measuring thickness is rough; however, its

main advantage is that it is in-situ method.

The normal mode of QCM used in the setup was at 5 MHz. The changes of frequency corresponding to 50 nm of deposited film were 100 Hz.

2.2.2 X-Ray Photoelectron Spectroscopy

X-Ray Photoelectron Spectroscopy (XPS) was measured in Phoibos 100 Specs detector. XPS allow us to determine the elemental composition, as well as to analyse the chemical bonds. The XPS uses x-ray radiation to generate photoelectrons. The photoelectrons are produced by interaction of x-ray photons with the specimen, where core level electrons are lost from atoms. These electrons have characteristic kinetic energy

$$KE = hv - BE - f \qquad 6)$$

where hv is the energy of the incident photons, BE is the binding energy of the electron and f is a work function of the spectrometer. The energy of incident photons depends on the type of the X-ray lamp. In our case, we work with an aluminium cathode, therefore, the characteristic peak is Al Kα [1486,7 eV]

The measured peaks in electron energy in comparison with tabulated binding energy of different atoms allows us to estimate the composition of the film. To obtain the relative contribution of these chemical species, the signal intensity must be normalised with relative sensitivity factor and the area of these peaks must be estimated.

The XPS is a surface characterisation method. The mean path of photoelectrons solids is a several nanometres, so most of the signal comes from about top 10 nm of the surface. From the deeper layers of the material the photoelectrons are scattered and lose their characteristic energy, they are therefore, measured simply as the background signal.

In our setup the anode was operated at the power of 200 W. The wide spectra were measured in an energy region reaching from 0 eV to 1100 eV using the pass energy value of 40 eV. High resolution spectra were collected using the pass energy of 10 eV with 10 scans for each peak. All measurements were performed under the ultra-high vacuum conditions under the pressure of 5.10^{-8} Torr. The films measured with XPS were deposited on silicon substrate with 1,5 nm of native silicon oxide layer. The usual thickness of the deposited film was 100 nm, such thickness allowed us to avoid the signal from Silicon background. [29]

2.2.3 Fourier-Transform Infrared Spectroscopy

Fourier-Transform Infrared Spectroscopy (FTIR) allows to characterize chemical groups composing the material. It uses absorption of infrared light at characteristic frequencies corresponding to vibrations of those chemical groups. In this work, Reflection-Absorption spectroscopy configuration was used on Bruker Equinox 55.

For these measurements, samples were deposited onto silicon substrates coated by a thin gold film. The measurement of background was carried out 3 times, and then 2 times the spectrum of the sample was measured. The resolution was set at 4 cm^{-1}.

2.2.4 Nuclear Magnetic Resonance

NMR allows us to assign in which chemical groups are hydrogens and This is based on measuring of the spin properties of hydrogens and 13C carbons, both with a spin ½. The spin system is manipulated by external magnetics field and magnetization is measured of nuclei. This interaction of external magnetic field and magnetization is described by Bloch´s equations. Resonance frequency of each nuclei is influenced by electron structure of its surroundings and it is shifted. By studding these chemical shift changes it is possible to distinguish between different chemical groups.

2.2.5 Gel Permeation Chromatography

GPC is a method for estimation of molar mass of measured polymer GPC separates the measured polymer by its hydrodynamic volume. The measured polymer permeate through the column with gel beads of 5 μm size. These beads have a pores. The smaller molecules diffuse through the system slower, therefore the distribution of molar mass can be estimated as distribution of elution time. The experiment were done using PLgel 100A/ 5 μm at flow 0.8 mL/min of the sample diluted in Tetrahydrofuran at 30°C.

2.2.6 Measurements of Wettability

The Water Contact Angle (WCA) method allows us to obtain information about the wettability properties of the film. The droplet of water placed on the surface takes the most energetically favourable shape with the characteristic contact angle between the surface and water. Therefore, it is possible to distinguish between a hydrophilic surface, i.e. the surface where the droplet spreads over the surface and the water contact angle is below 90º and hydrophobic (non-wetting), where the water angle is over 90°

The contact angle can be changed by two main properties of the surface, the roughness of the film and the surface energy. In this the surface energy was modified by changing the chemistry of the film. Typically, polymeric films with more oxygen have higher surface energy and are more hydrophobic. The WCA was measured three times to acquire statistics.

2.2.7 Spectroscopic Ellipsometry

Spectroscopic ellipsometry is a contact free method used to determine the thickness and optical constants of the films. The change of the light polarisation between the well-known polarization of incidence light and the measured refracted light is measured. The change in the ratio between the s and p polarization of refracted light is observed and their phase shift is measured. These two parameters are called Ψ and Δ. These data must be fitted according to the constructed model to obtain optical constants and thickness of the sample. An optical model suitable for thin transparent polymeric films is a simple Cauchy model. This model describes the properties of refractive index *n* on the whole measured range with four parameters.

$$n(\lambda) = A + \frac{B}{\lambda^2} + \frac{C}{\lambda^4} \qquad 7)$$

,

A, B, C and the index of absorption k is fitted by Urbach absorption term.

The Woollam M-2000DI spectroscopic ellipsometer was used in this study. The measurements were performed on about 100 nm thick films, deposited on polished silicon. The measurements were done at three angles from 50° up to 70° and in the wavelength range of 192 nm - 1690 nm. The ellipsometry data were fitted using a CompleteEASE software (J.A. Woollam) according to Cauchy model for silicon substrate with 1.5 nm of native oxide.

The in-situ measurements in water were done in a flow cell. The angle of measurements was 70°, because of the geometry of the flow cell. The in-situ data were fitted by Bruggeman effective medium approximation model, where the medium was water and the inclusion were the layer described by Cauchy model.

2.2.8 Scanning Electron Microscopy

Scanning electron microscope (SEM) is an imaging technique enabling us to study the topography of a sample by scanning the surface with a focused beam of electrons. The high energy electrons (0,2 – 40keV) emitted by field emission gun are focused a with set of lenses on a tiny spot. The interaction of these electrons with the surface results in multiple effect, i.e. the emission of secondary electrons, backscattered electrons, generation of X-ray etc. The intensity of these emitted electrons and X-rays depends on the morphology and chemical compound of the surface. These signals can be obtained by different types of detectors at different positions in the microscope. By scanning with primary beam it is possible to obtain the resulting raster image.

The SEM in this thesis was used in the simplest mode. We used only the secondary electron detector. The acceleration voltage was set at 1 KeV. The area of the measured view fields was 60x45 μm.

2.2.9 Hydrolysis

The hydrolysis characterisation allows us to estimate the chemical stability of the films. The chemical reaction, where the PLA molecule is shortening is observed. A hydrolysis test was carried out in demi water (enriched with 0.2 %wt. sodium azide) on square shaped glass samples (2.5x2.5 cm) that were previously treated with PAVTD plasma deposition. The specimens were immersed into hydrolysis medium (at the temperature of 37°C) placed in 20 ml weighing bottles and shaken. At defined time intervals, 1 ml was withdrawn for LC-MS analysis that was performed on an Infinity LC System (Agilent Technologies, USA). Chromatographic separation was performed on an Extend column C18 (2.1x50mm, 1 um) at the flow rate of 0.5 mL.min-1. The mobile phase consisted of 0.1% formic acid (A) and acetonitrile (B), the sample injection volume was 1 uL. Standard of lactic acid was measured as a [M-H]- molecule ion, fragmentation of the precursor ion was carried out at 20 V.

2.2.10 Permeability

In order to characterise the barrier layers properties, the permeation test can be done.

The time of permeation of active model molecule is characterised. Permeability was tested by using active molecules of different molar weight (nisin-N, cetyl pyridinium bromide-CPB, bovine serum albumin-BSA, sodium salicylate-SS). Active molecule-containing layers were prepared via spin coating (3000 rpm) of the polyvinyl alcohol

(2%wt.) solution with an active substance (1%wt.), the total volume of 450 mL, on silicon wafers (2.5x2.5 cm). Subsequently, PLA-like PAVTD polymer layer (thickness ~100 nm) was deposited on the substrates.

The samples containing the layer of active sample and PLA thin film were immersed into demi water (at the temperature of 37°C) in 20 ml weighing bottles and shaken. At defined time intervals, 1 ml was withdrawn for further analyses.

Detection of nisin was performed on a HPLC Shimadzu Prominence LC20A Series equipped with thermostatted column compartment and a dual wavelength UV-VIS detector (Shimadzu, Japan). The measurement was performed on an Aeris Widepore column XB-C8 (4.6x150mm; 3.6 um; Phenomenex, USA) at 40°C. The mobile phase constituted a gradient composed of 0.1% (v/v) HCOOH in HPLC grade water (solvent A), and HPLC grade acetonitrile (solvent B). Gradient elution was as follows: 0–13.5 min, from 5.0% eluent B to 40.0% eluent B; 13.5–14.0 min, from 40.0% eluent B to 95.0% eluent B; 14.0–18.5 min, 95.0% eluent B; 18.5–19.00 min, from 95.0% eluent B to 5% eluent B; total run 25 min. Injection volume equalled 40 μL, and the flow rate was set to 1.00 mL/min. Measurement was performed at the wavelengths of 200 and 220 nm; the concentration of nisin was calculated from the results of the 200 nm test. Quantification of nisin was performed by external calibration method and the equation of calibration curve was the following: $y = 137970c + 159{,}26$ ($R^2 = 0.9992$), where y represents the peak area and c the concentration of nisin.

Detection of CPB and SS was performed by measuring the absorbance on a WTW photoLab 6600 UV-VIS spectrophotometer. SS was analysed using the 5mM $Fe(NO_3)_3$ in 12 mM H_2SO_4 reagent at pH 2.5 (515 nm). Detection of CPB was performed using bromopyrogallol red (BPR) agent and $SrCl_2.6H_20$ solution in acetate buffer at pH 4 (584 nm).

2.2.11 Substrates

The films were deposited on several different substrates. The films prepared for XPS, FTIR, ellipsometry, WCA analysis were deposited on single side polished silicon wafers with size 1x1 cm. Films for FTIR was measured on silicon covered by 100 nm thick layer of gold. For the permeation tests the active molecules film were deposited by spin-coater on single side polished silicon and subsequently the PLA-like film were deposited. The samples for hydrolysis were deposited on glass substrate with size 2.5 x 2.5 cm The

samples for NMR and GPC analysis were deposited on glass plate with size 20x20 cm. The film was subsequently removed from substrate with razor and collected into vial, where was characterised.

3 Experimental Part

3.1 Development of the PAVTD Setup

The brief concept of PAVTD was shown in chapter 1.6 Plasma Assisted Vapour Thermal Deposition. The aim of this chapter is to introduce our actual setup and its properties. The configuration was changed several times during work on this thesis. The development can be divided into three steps.

In the first step we used the original setup previously used for preparation of PEO. In this setup the classical planar RF electrode was placed under the heating cell. Therefore, the precursor polymer was evaporated above the plasma in the afterglow region. No electronic was used to control the deposition conditions. The temperature of heating cell was manually controlled by changing the current through the ohmic heating wires.

In the second step, the first attempt was made to control the deposition process with electronic. However, the RF disturbance of the electronics were high. At higher plasma powers the electronics did not work. It was possible to controllably produce only samples up to 20W of plasma power.

The results of the deposition process depend on many parameters, the most important being plasma power. However, the results are also influenced by the deposition rate and evaporation temperature. In the first attempt the temperature was kept constant. This led to very broad differences of deposition rates for different samples, because the deposition rate was decreasing with deposition time at a constant temperature. It was possible to partly correct by introducing Yasuda-like parameter and concept of effective power – power divided by flow rate.[30] The actual model of this setup is depicted in figure(10).

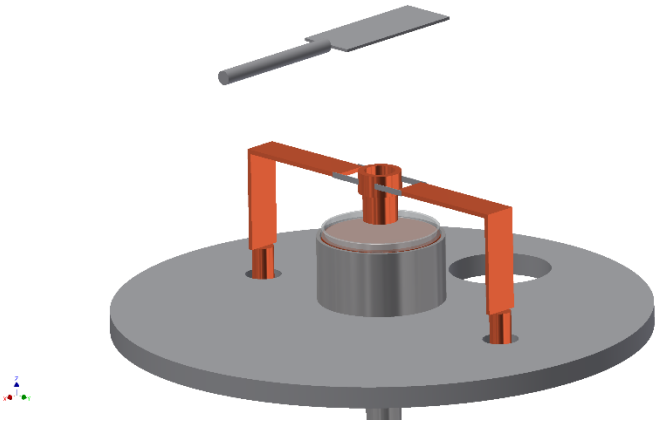

Figure 10. *experimental setup of PAVTD with planar electrode Q – substarte holder T – heating cell M – planar electrode*

In the second step we rearranged the deposition setup to decrease the RF disturbance. Instead of the planar electrode we placed a the cylindrical antenna above the heating cell. This increased the distance between the electrode and temperature sensor which was mainly influenced by RF disturbance. Instead of a constant temperature we kept a constant deposition rate. RF disruption was still high, therefore, it was decided to control the deposition rate via temperature manually. The setup is shown at figure (11).

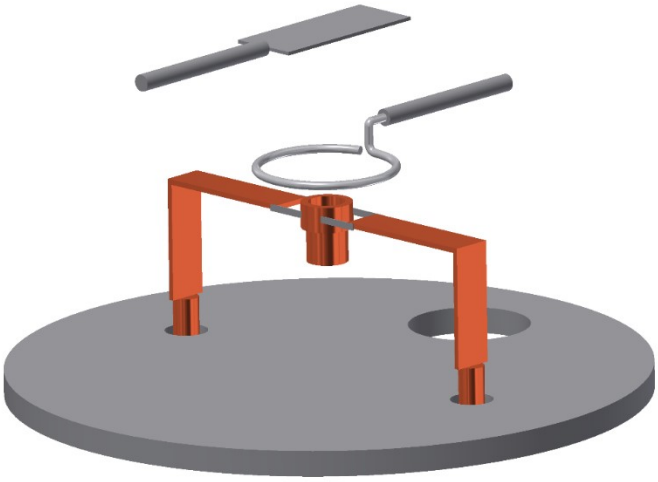

Figure 11. *experimental setup of PAVTD with antenna Q – substarte holder T – heating cell M – antenna*

In the last step we improved the RF shielding of the electronics. The controlling software developed by Pavel Solař was also improved in order to keep the deposition rate semi-constant. The geometry of the setup remained same as in the second step.

Deposition rate in final setup was around 5 nm per minute in all cases. During deposition the heating cell was heated to higher temperatures to keep deposition rate constant. The samples were prepared between the temperature of 220°C and 300 °C. With manual control of the temperature, it was possible to keep the deposition rate almost constant. Around 300 °C we observed a rapid increase of the deposition rate, therefore we tried avoid this regime. Using a simple feedback algorithm of the deposition rate we obtained semi-periodical deposition. This can be seen on figure (12). In the figure the measured parameters – deposition rate, pressure and temperature - for one deposition are shown.

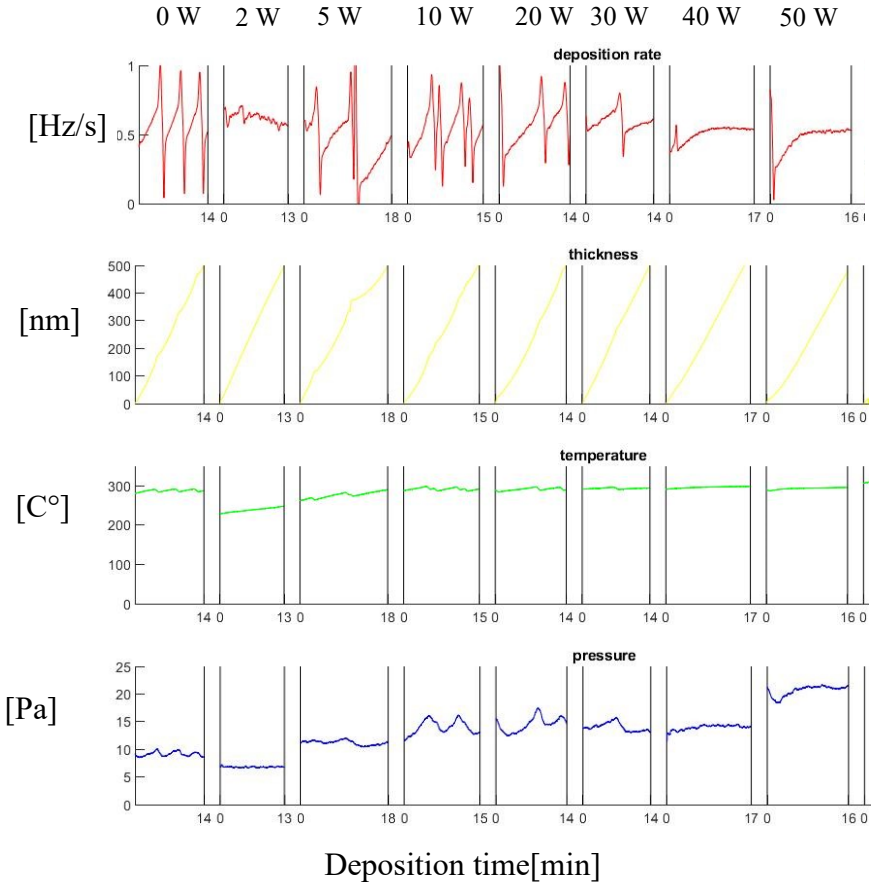

Figure 12. *The deposition conditions red- deposition rate, yellow thickness, green temperature, blue – pressure for 0 – 50 W of plasma power.*

We prepared two kinds of deposits. In the first case we needed to deposit as much material as possible for the NMR and GPC characterisation. In this case a glass plate with

a size of 20x20 cm, was used as substrate. This plate was put in a vacuum chamber before the deposition. The power introduced to plasma was kept constant. The deposition rate grew till 200 °C and then was kept constant during the whole deposition.

In the second case we needed around 100 nm thick films for ellipsometry, XPS, FTIR and other characterisation techniques. As the time window of constant deposition rate was between two to four hours and deposition time of 100 nm was around 20 minutes, it was possible to prepare several samples during one deposition. Sets of samples varying in the power were produced in this way. We were able to produce four to six samples during one deposition from one fill of the crucible. The samples prepared at higher powers were prepared later during the deposition. This was decided in order to avoid loss of the whole deposition time in case the electronics stopped working due to RF disturbance this led to systematic error due to the correlation between the serial number of sample and power. After several checking experiments we consider that the errors which arose from other parameters are of higher significance.

The whole setup is placed in a vacuum chamber. The chamber is firstly evacuated to the 10^{-2} Pa. Then the flow of working gas is adjusted to keep during the experiment the pressure of 3 Pa in the chamber. The working gas is an Argon. The vacuum chamber is pumped whole time during experiment by a diffusion pump and a rotary pump. The RF electrode is powered by xxx power supply in the range of 0-150 W. The frequency of RF is 13.56 MHz.

3.2 Data Sets

A total of eight sets of samples varying in plasma power are presented in this paper. The list of sets shown in this paper and the techniques employed for characterisation are depicted in the next table (1).

deposition setup			characterisation techniqes									
set	power [W]	numberof samples	XPS	FTIR	NMR	ellipso - thickness	ellipso - swelling	ellipso - disolving	WCA	GPC	hydrolisis	permeation
A	0-100	13	x	x		x	x	x	x			
B	0-20	6	x	x		x	x	x	x			
C	0-50	8	x	x		x	x				x	
D	0-120	10	x	x		x	x	x	x			
E	0-100	5/29	x		x							
F	0-20	6	x	x		x						
G	0-150	16	x	x		x			x			
H	0-100	10	x	x		x			x			x
I	0-50	5	x	x						x		

Table 1. *The list of prepared sets of samples with characterisation techniques employed for analysis*

Set A was prepared using the original setup with planar electrode. The results from this set were published in [30]

Set B was the first attempt to prepare samples with cylindrical electrode.

The main use of set C was in the analysis of hydrolysis.

Set D is the main data set for overall performed analysis. This set was still controlled manually. However, it achieved a relatively good reproducibility.

As of this point, all remaining series were prepared with automatic deposition control.

Set E was prepared for NMR analysis. Each of five powers were prepared from one whole deposition. Several short-term samples were prepared during these depositions. The main

aim of these samples was to show that the sample index and temperature at which the sample was deposited was insignificant.

Set F was prepared with different flow rates to verify the influence of Yasuda parameter.

Set G was done in order to check the deposition parameters for set H. As it was performed with the same parameters as set H it can be used for verifying the of reproducibility of the PAVTD process.

Set H is the second main data set. The characterisation of permeation was done on samples from this set

Set I was done for GPC analysis. It was performed-like set E (i.e. the NMR set)

3.3 Chemistry of PAVTD PLA Layers

3.3.1 Fourier Transformer Infrared Spectroscopy

The FTIR was measured on 100 nm films on gold-coated substrates were characterised in reflection-absorption mode. The results were recalculated to the absorbance. The measured data were compared with results reported in the literature, especially the paper [AF], in which they synthetized PLA-PEG by a classical wet chemistry method and analysed their samples by FTIR and Raman spectroscopy.

Interestingly, we observed similar changes in FTIR spectra measured on our samples. Especially, the relative increase of the aliphatic CHx vibrations signal in 2800-3000 cm^{-1} region was substantial.

The graph with FTIR results from the paper [31] was reprinted in the figure (13).

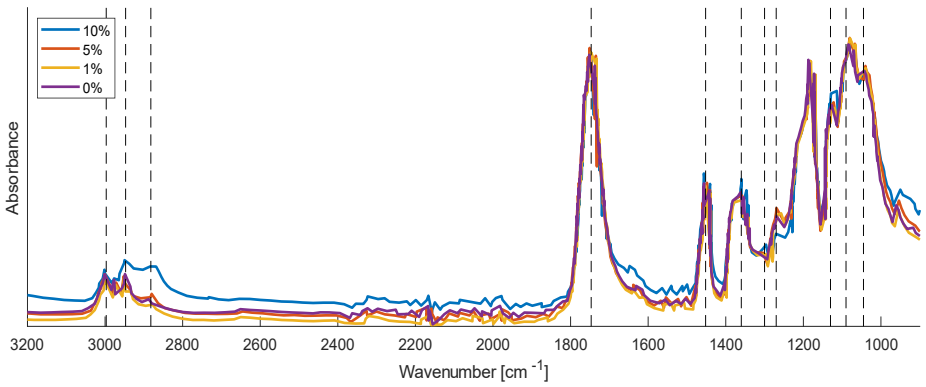

Figure 13. *The FTIR spectra of PLAPEG prepared by wet chemistry method. The ratio of PEG compound increases from 0% up to 10%. The graph is reprinted from [31]*

Our measured data are shown in graph (14). The spectra are normalized to the vibration of C=O 1747 at cm^{-1}. The gradient of colour discriminates different plasma powers. The assignment of the peaks was taken from [31]

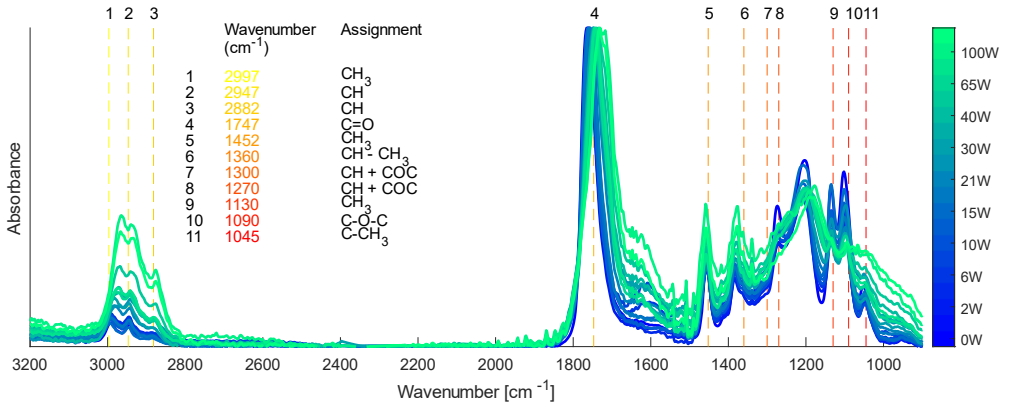

Figure 14. *The FTIR spectra of PLA thin films prepared by PAVTD. The colour gradient distinguish between samples varying in the power of plasma used for preparation. The FTIR spectra are normalized in C=O vibration (1747 cm^{-1})*

All of the samples prepared with different plasma powers have typical peaks of the conventional PLA in FTIR spectrum, only the relative intensities change. Namely, we spotted an increase in 2800-3000 cm^{-1} region, where functional groups like methyl can be found.

The C=O peak moved from 1765 cm^{-1} for 0 W up to 1730 cm^{-1} for 100 W, which was caused by changes in chemical environment surrounding the C=O bond with possible influence of C=C bonds that can be responsible for the increase of absorption near 1650 cm^{-1} with increasing plasma power.

In the region from 1500 cm^{-1} to 1000 cm^{-1}, we saw a slight increase of CH vibrations.

Because of the similar thickness of layers which varied in the range of 80-120 nm, it was possible to renormalize the spectra by the thickness with a simple formula:

$Absorbance_{(thickness)}$ = Absorbance/thickness

The renormalized graph is shown in figure (15).

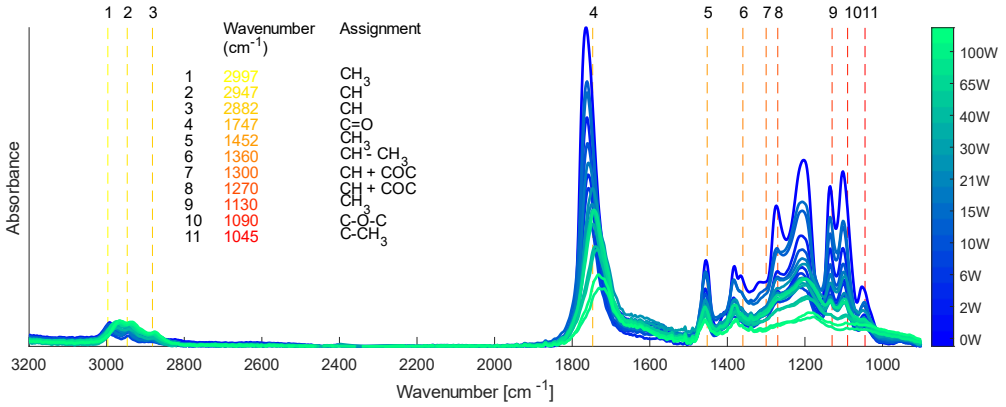

Figure 15. *The FTIR spectra of PLA thin films prepared by PAVTD. The colour gradient distinguish between samples varying in the power of plasma used for preparation. The FTIR spectra are normalized on the absorbance in dependence of thickness*

In this way it is more clear that the most important change is the lost of oxygen containing groups.

3.3.2 Notation

The results from XPS and NRM analysis and chemical model are going to be presented in the next chapters. In order to compare data from these techniques, careful notation of various chemical groups must have been made.

We think that several different structures are formed in films. Namely ester chemical groups- original PLA, ether chemical groups and carbon rich parts. However, this notation would not be sufficient for NMR and XPS analysis as chemical bonds are characterised. Choosing a model polymers (PLA, PEG, PP) was also tried, but using just this notation is misleading as it cannot be said that exactly these structures are formed. The table (2) shows the used notation for different techniques and purposes. The notation in each column corresponds to “similar chemical structure” The author realise that the used notation is not ideal, but he was not able to find suitable notation for all cases.

XPS notation	C1 (C-C)			C2.1 (C-O-C)	C3 (O-C=O)	O1 (O=C-O)	O2.1 (C-O-C)	C2.2 (C-O-C)	O2.2 (C-O-C)
XPS "official fitting notation"	PLA C1			PLA C2	PLA C3	PLA O1	PLA O2	PEG C2	PEG O2
XPS binding energy BE(eV)	285			286.98	289.06	532.25	533.66	286.45	532.83
NMR notation	PLA CH_3	CH_3	CH/CH_2	PLA CHO				CHO/CH_2O	
NMR recalculated on carbon	PLA CH_3	CH_3	CH/CH_2	PLA CHO				CHO/CH_2O	
NMR chem. Shift(ppm)	1.5	0.7-1.4	1.9-2.7	5.1				3.9-4.3	
Model polymer structure	PLA	PP	PP	PLA	PLA	PLA	PLA	PEG	PEG
Chemical structure – "Notation used in thesis"	ester	Carbon-rich-polymer	Carbon-rich-polymer	ester	ester	ester	ester	ether	ether

***Table 2**. Used chemical notation*

3.3.3 X-Ray Photoelectron Spectroscopy

3.3.3.1 XPS - Tabulated Data

The XPS Survey, C1s and O1s spectra were obtained. The analysis of these spectra was done in CasaXPS software. The measured data were compared with the XPS of polymers database [32]. The tabulated decomposition of PLA are shown below in figure(16).

a)

Poly (d,l-lactide) (PLA)					
	C 1s			O 1s	
	C 1	C 2.1	C 3	O 1	O 2.1
BE(eV)	285	286,98	289,06	532,25	533,66
FWHM(eV)	1,19	1,07	0,97	1,23	1,31
Area(%)	36	33	31	50	50

b)

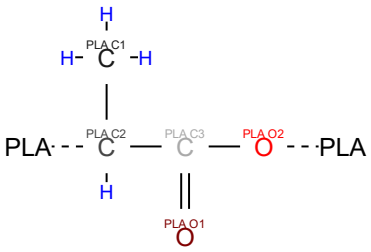

c)

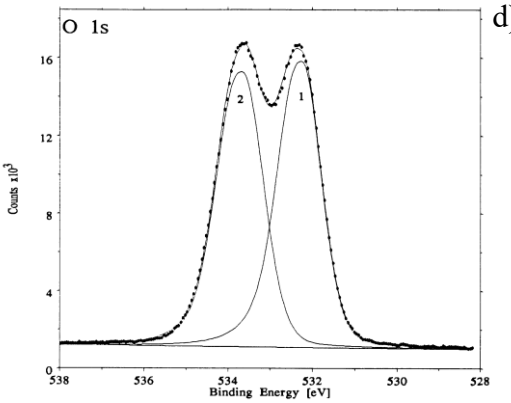

d)

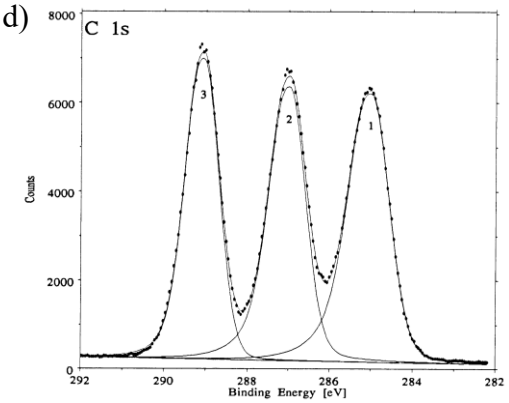

Figure 16. *a) XPS tabulated data of PLA b) structural formula of PLA c) XPS O1s high resolution peak of PLA d) XPS C1s high resolution peak of PLA*

It was found that fitting the data with PLA peaks alone does not fully describe the measured data.(see below) and we had to introduce some C-O-C structures to our fitting. We chose the PEG as a model polymer of these structures and took its chemical XPS shifts. The XPS parameters for PEG are shown below in figure (17):

a)

Poly (ethylene glycol) (PEG)		
	C 1s	O 1s
	C 2.2	O 2.2
BE(eV)	286,45	532,83
FWHM(eV)	1,05	1,21
Area(%)		

b)

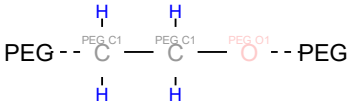

c)

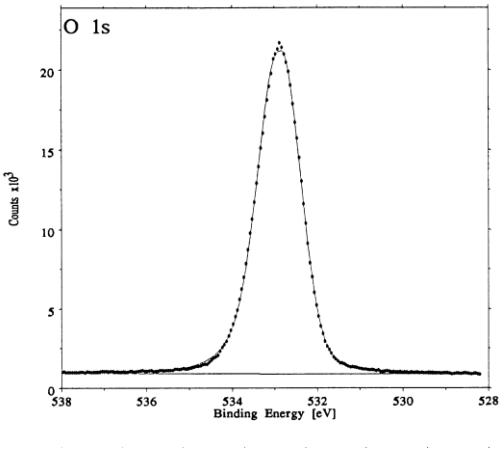

d)

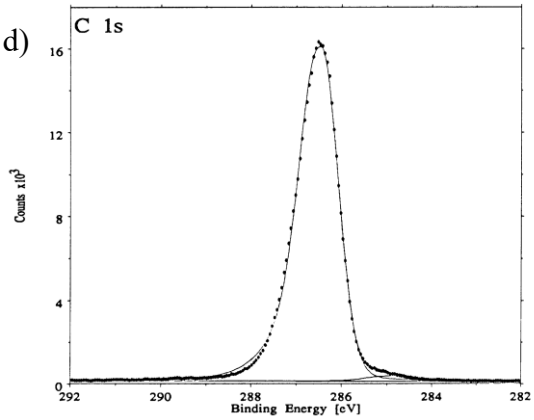

Figure 17. *a) XPS tabulated data of PEG b) structural formula of PLA c) XPS O1s high resolution peak of PEG d) XPS C1s high resolution peak of PEG*

3.3.3.2 XPS - Measured Data

Overall, more than 50 samples in the range between 0 and 150 W were characterised by XPS. To keep the characterisation and visualisation more simple only set D containing 20 samples was chosen to be shown here. All of the samples for XPS were prepared on silicon substrates. The typical thickness of these layers was 100 nm. This is sufficient thickness to restrict the signal from the background of the silicon. However, some silicon around 0-5% was measured in our samples prepared at the lowest plasma powers (<20W). We assume that this is caused by an inhomogeneity of the films. It has to be pointed out, that the presence of the silicon influences the results measured with XPS not because of

the silicon, which can be neglected, but because of the presence of oxygen in SiO_2 , which cannot be distinguished from oxygen in the hydrocarbons.

The measured high resolution spectra of carbon and oxygen are shown below a in figure (18). The measured intensity of oxygen was multiplied by the relative sensitivity factor to obtain the comparable areas of carbon and oxygen peaks in the graph. The theoretical binding energy position of bulk PLA peaks are added in the graph. The parameter of power is shown as a gradient in colour. The oxygen parts of spectra were recalculated with relative sensitivity factor of oxygen, so the ratios between fitted peaks match the ratios between contributions.

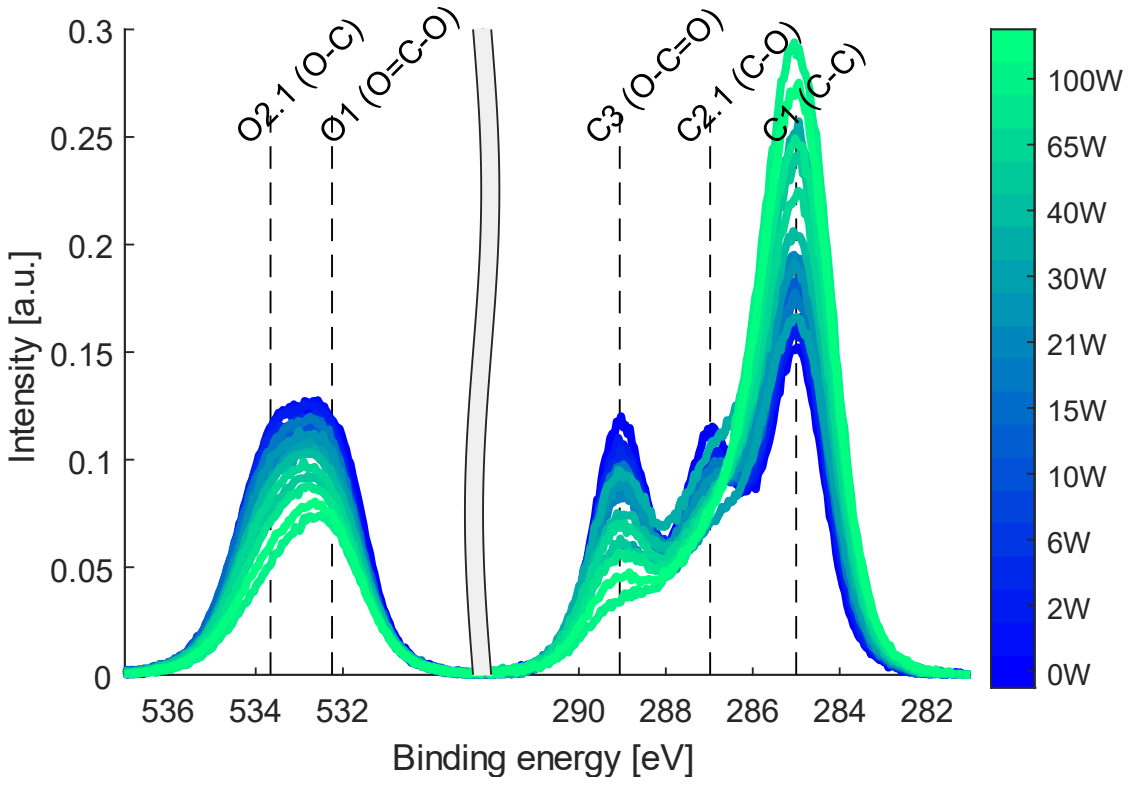

Figure 18. *The measured XPS spectra. The colour gradient distinguish between samples varying in the power of plasma used for preparation. O1s part rescaled by relative sensitivity factor. The overall area of C1s and O1s is renormalized on 1 for all plasma powers.*

One obvious trend can be seen in the raw data without any deeper analysis of relative increase of the PLA C1 peak. This peak is related to aliphatic carbons in PLA and also to all the other aliphatic carbon atoms present in the samples.

3.3.3.3 XPS Fitting - PLA Peaks Only

The data were at first fitted by tabulated PLA structure. The positions of three carbon peaks were set at 285, 286.96 and 289.06 eV. The energy difference of oxygen peaks was set to 1,21 eV. The position of O1 oxygen peak with respect to C1 carbon peak was a fitting parameter. All the other parameters – FWHM and the area for all peaks were set as the fitting variables. The comparison between measured data and an envelope curve of the fit is shown below in figure (19).

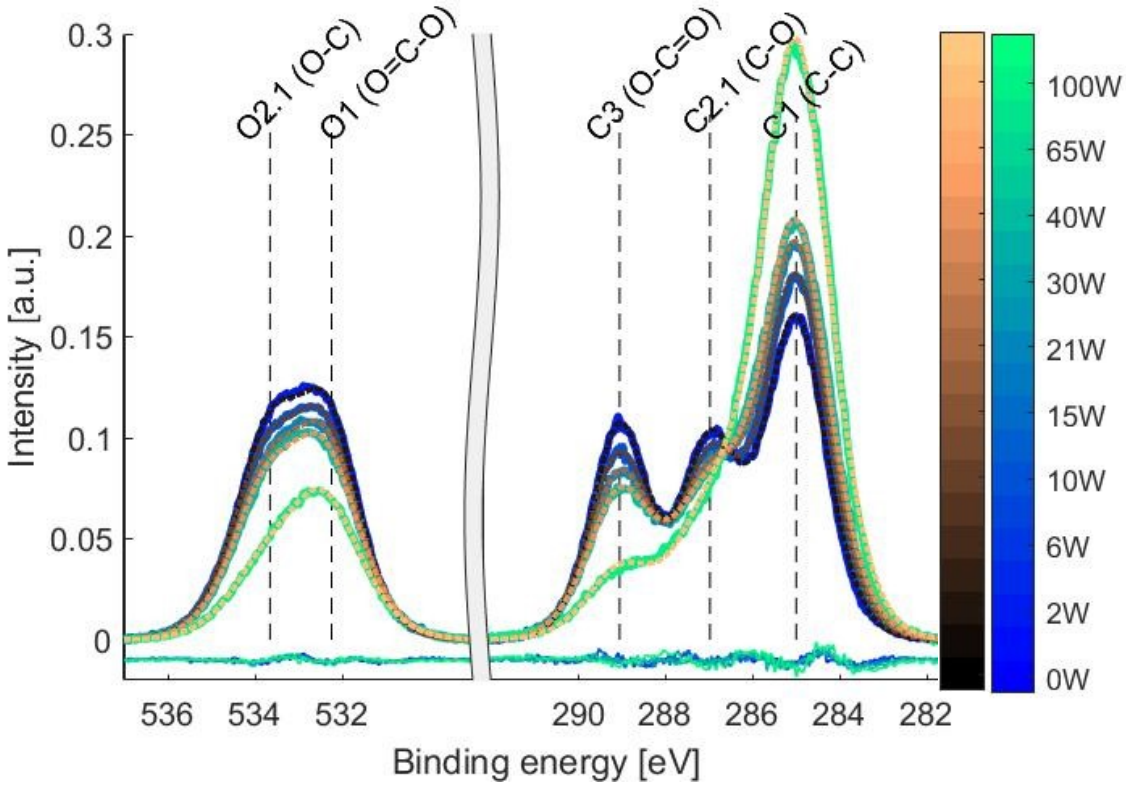

Figure 19. *The comparison between measured XPS data (blue-green colour gradient depicts plasma power used for preparation sample) and fit (black-bronze colour gradient) with just PLA structure. The difference between fit and measured data is shown below the comparison with offset. The actual fit decomposition can be found on figure 20.*

The fitted curve with pure PLA structure visually describes pretty well the measured data especially for lower powers of plasma. The actual decomposition is shown below in figure (20).

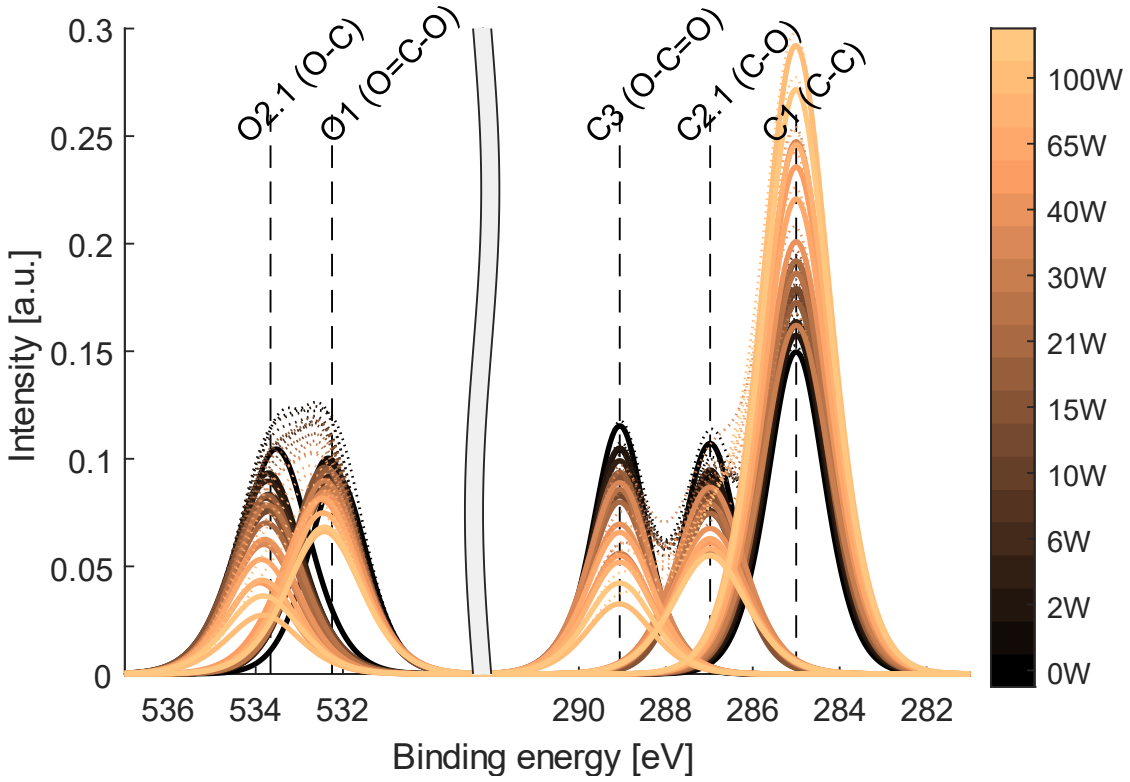

Figure 20. *The decomposition of fit with just PLA structure. Black-bronze colour gradient distinguish plasma power used for preparation.The dashed lines are the envelope curves on fit. The C1, C2.1, C3, O1, O2.1 are tabulated energetic position of PLA peaks*

The analysis of these XPS spectra suggests two trends .Firstly, the PLA C1 peak grows with increasing intensity of plasma. Secondly, the PLA C2.1 (**C**-O-C) peak and PLA O1 (**O**=C-O) peak seem to exhibit a similar decrease with respect to plasma power. The same dependence of intensities was observed for PLA C3 (O-**C**=O) and PLA O2.1(C-**O**-C) peaks, but the rate of change was bigger. This correlation of C2.1(**C**-O-C) and O1(**O**=C-O) and on the other hand PLA C3(O-**C**=O) and PLA O2.1(C-**O**-C) looks chemically very strange as the PLA C3(O-**C**=O) and PLA O1(**O**=C-O) peaks should have the same intensity, because the amount of carbon doubly bonded to oxygen has to be the same as oxygen doubly bonded to carbon. The actual dependence of chemical composition of power is depicted in figure (21).

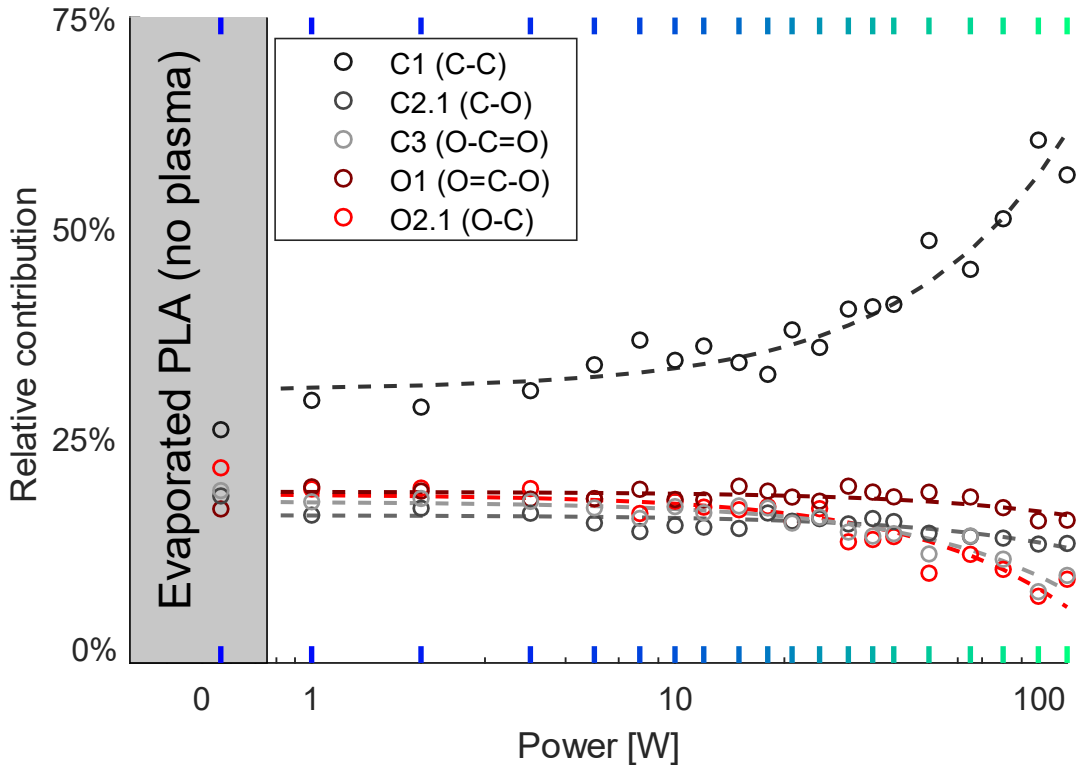

Figure 21. *Chemical composition according to XPS (fitted with just PLA peaks) in dependence on plasma power used for preparation of samples The C1, C2.1, C3, O1, O2.1 corresponds to tabulated PLA peaks*

We think, that this chemical imbalance is caused by incompleteness of the fit. There can be other peaks, which are wrongly interpreted as part of ester PLA peaks in this model.

XPS fitting – with ether bonds.

It was found that adding ether peaks can fix this imbalance. The chemical shift of carbon for such structure is between 286.13 – 286.75 eV and for oxygen between 532.47-532.83 eV. We did not want to add the position of these ether peaks as a fitted parameter so we chose the PEG as model polymer and set the position of new peaks as it would be in PEG. It has to be pointed out that we do not think that PEG structure is formed in structures. The binding energy for carbons in PEG is 286,45 eV. This is close to 286,98 eV for C-O-C in PLA groups. On the other hand, the binding energy for oxygen in PEG structure is 532,83 eV This energy is closer to binding energy of PLA O1 (O=C-O) (532,25 eV), than to binding energy of PLA O2.1(C-O-C) (533,66 eV). The ether PEG-like peaks take

from XPS point of view mainly contribution from PLA C2.1(C-O-C) and PLA O1(O=C-O) peaks. This behaviour is schematically shown in figure (22).

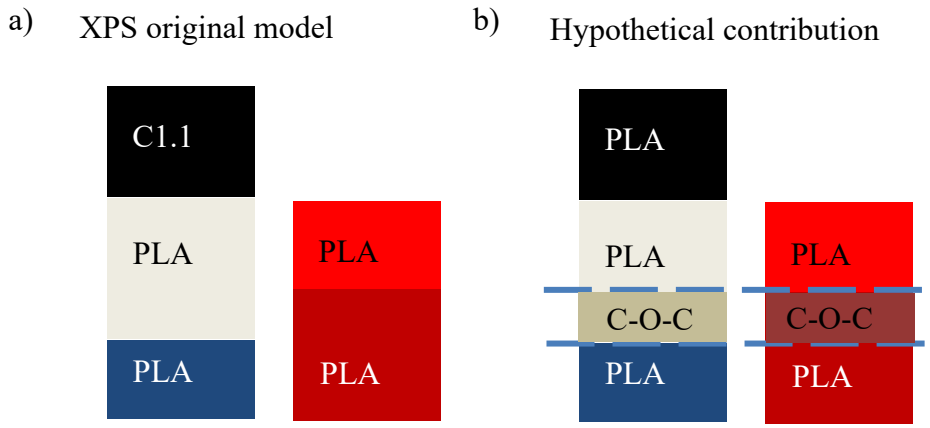

Figure 22. *The XPS model consisting just PLA structure do not correctly assign the C-O-C structures. a) model b) hypothetical structure*

To verify this idea, we modified the original fit and added the position of PLA C2.1(**C**-O-C) peak as a fitted parameter. Then we studied the changes of binding energy and FWHM with respect to plasma power. This is shown in figure (23)

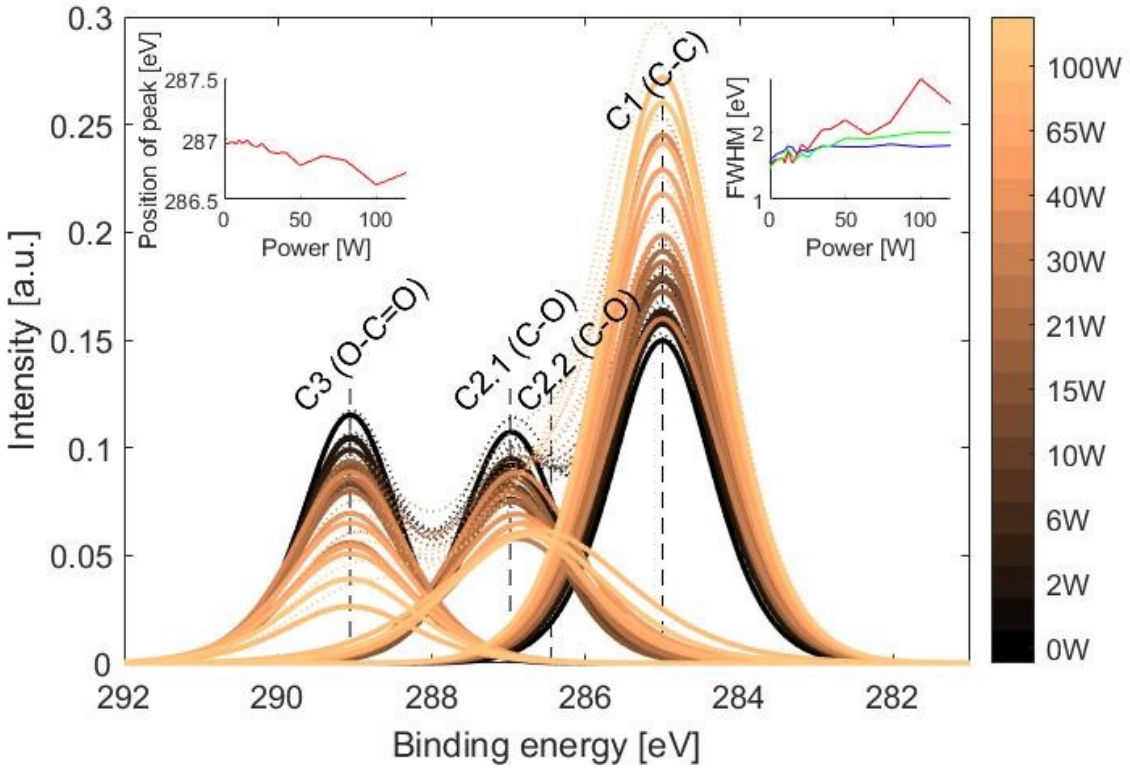

Figure 23. *The decomposition of fit with fitted energy position of C2.x peak. Black-bronze colour gradient distinguish plasma power used for preparation. The dashed lines are the envelope curves on fit. The C1, C2.1, C3, O1, O2.1 are tabulated binding energy of PLA peaks and C2.2 is tabulated peak of PEG*

It can be clearly seen that the position of the peak is shifting to lower binding energies with increasing plasma power. This suggests the presence of two peaks. The FWHM also increase with power and above 30W is higher than 2 eV. The real energy resolution of our XPS setup suggests that if peak has higher FWHM than 2 eV, it should be fitted with two peaks.

For this reason, we added the ether peaks in the final fit. This was easily possible for carbon part of the spectra. However, there were too many peaks for the oxygen part of the spectra. The fit became numerically instable, because there were too many fitting variables. This was fixed by assuming the same contribution of carbon doubly bonded to oxygen as oxygen doubly bonded to carbon. Firstly, the carbon part of spectra had been fitted. Then the area of PLA O1 (O=**C**-O) was set to be the same as the fitted area of PLA C3 (O-**C**=O). Lastly, the rest of oxygen peaks were fitted.

The results of this fit are shown below.

Firstly, there is comparison between the measured data and the envelope curve of the new fit. (Figure (24))

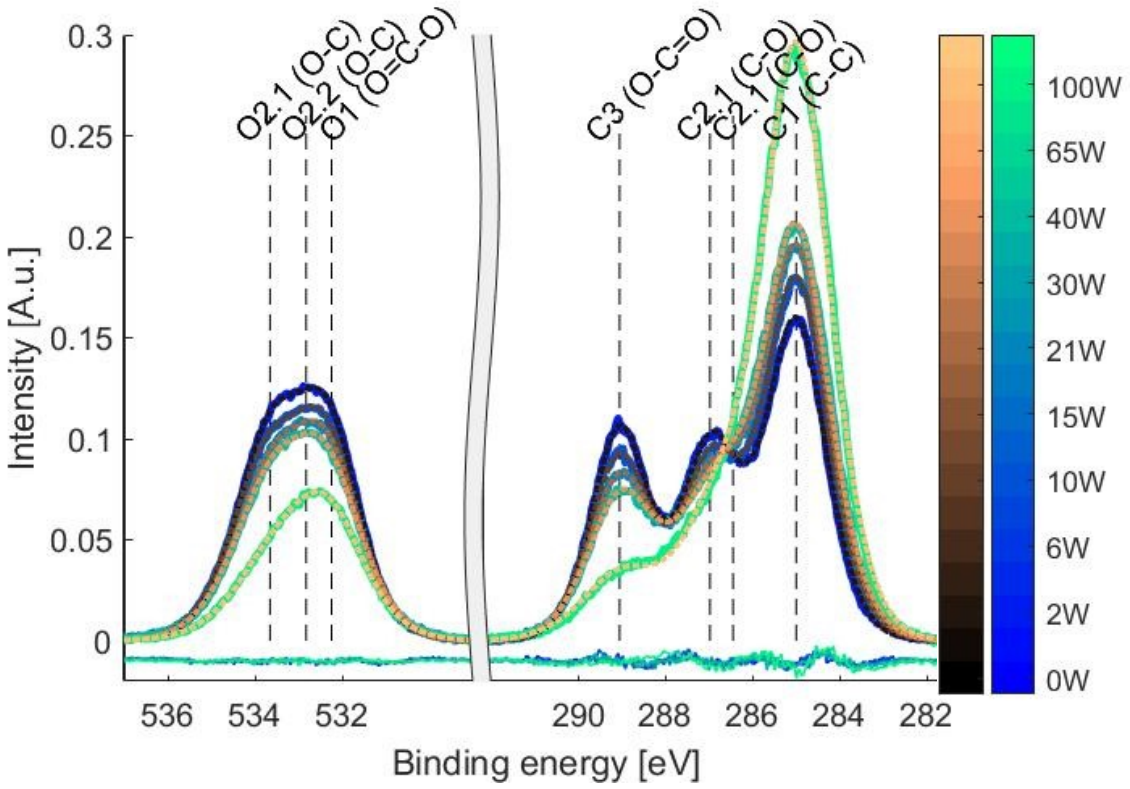

Figure 24. *The comparison between measured XPS data (blue-green colour gradient depicts plasma power used for preparation sample) and fit (black-bronze colour gradient) with PLA and ether structure. The difference between fit and measured data is shown below the comparison with offset. The actual fit decomposition can be found on figure 25.*

The actual decomposition is shown below in figure (25).

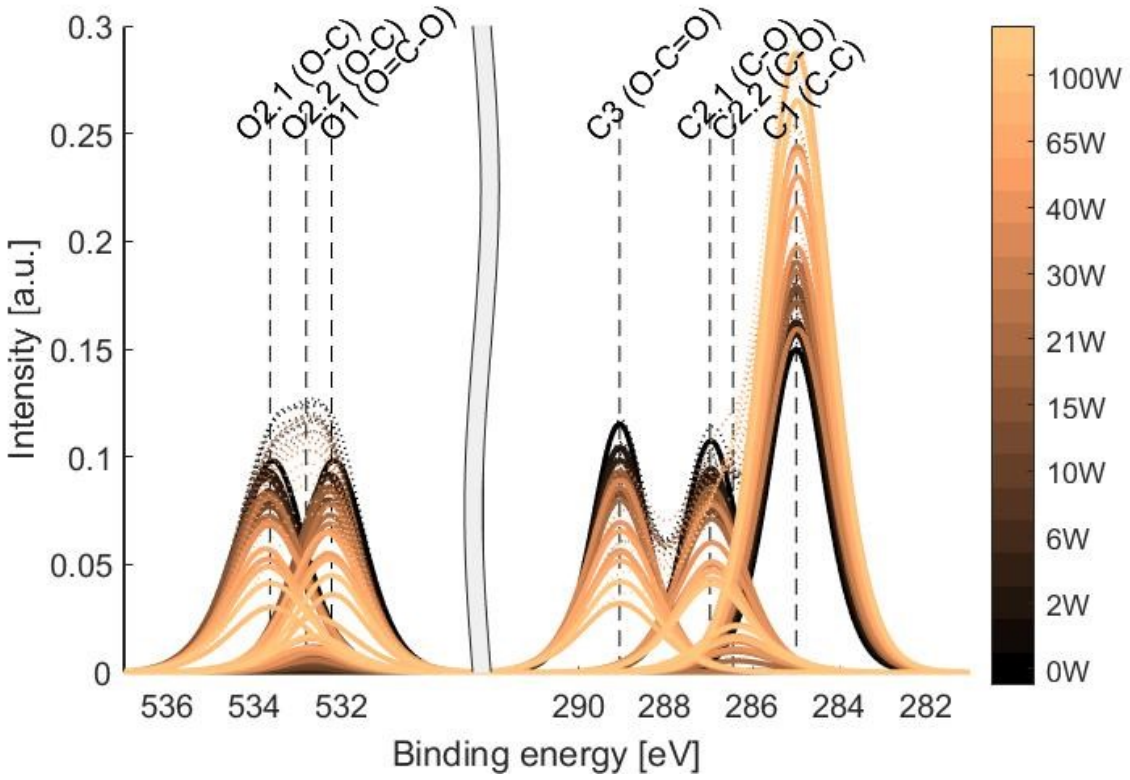

Figure 25. *The decomposition of fit with PLA and ether structure. Black-bronze colour gradient distinguish plasma power used for preparation. The dashed lines are the envelope curves on fit. The C1, C2.1, C3, O1, O2.1 are tabulated binding energy of PLA peaks, C2.2 and O2.2 are PEG peaks*

The areas of all peaks were calculated and the relative contribution of each compound was estimated. The results are shown in figure (26)

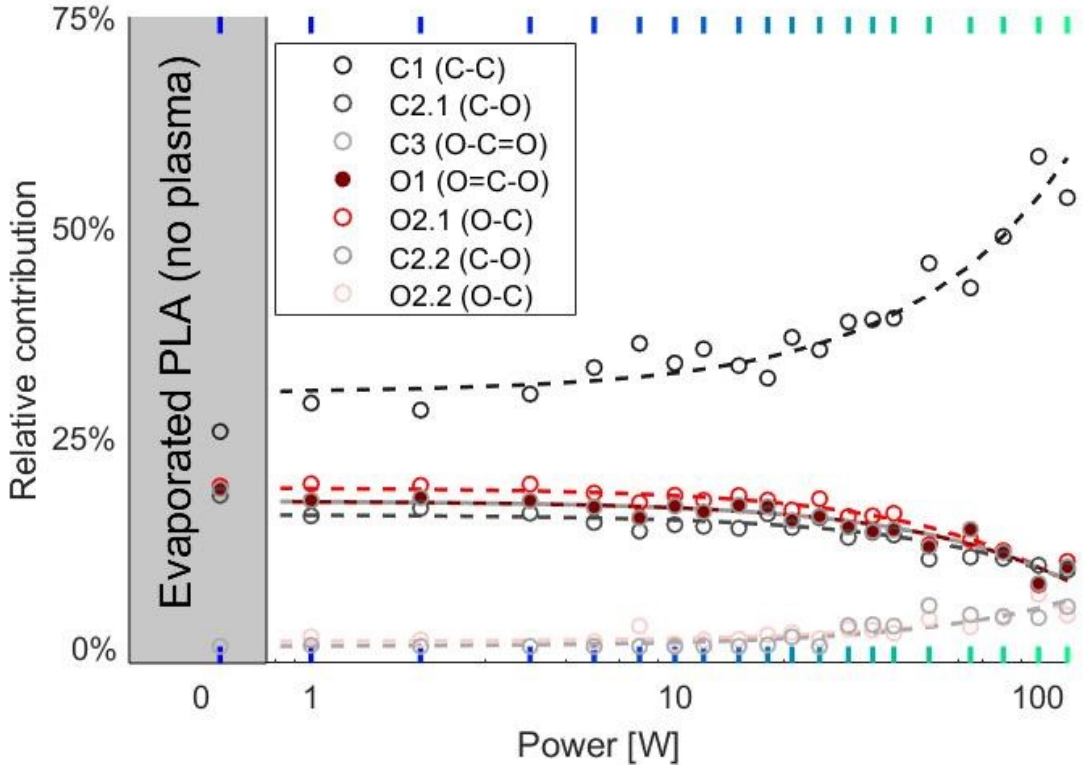

Figure 26. *Chemical composition according to XPS (fitted with PLA and ether structure) in dependence on plasma power used for preparation of samples The C1, C2.1, C3, O1, O2.1 corresponds to tabulated PLA peaks*

The PLA C3 and PLA O1 peaks have same area. As was described before this is not the result of fit but of our assumption and input in the fit. The new result is that the areas of PLA C2.1(**C**-O-C) peak and PLA O2.1 (**C**-O-C) peak have similar area, which varies in the range of 5 %. Moreover, these two peaks have also similar areas as PLA C3 (O-**C**=O) or PLA O1(O=**C**-O) for all powers. It means that at least part of the PLA chains was not fragmented and some of the original PLA structure is well preserved in the films. This fraction is decreasing with the plasma power. On the other hand, the contribution of PLA C1 increases with plasma power. There is not enough place for these aliphatic atoms in the PLA structures so these carbon atoms have to form some carbon rich part of the polymeric chains. The ether structure is formed in the films. The amount of this chemical groups increases with plasma power. The relative contribution of the XPS peaks is shown in table (2). These data were fitted by linear function.

$$C(W) = a + b.W\ ,$$

Where C is chemical composition, a and b are fitted parametrs and W is plasma power Those linear fits are shown as dashed lines in graph (26). The fitted parameters of the linear fit are shown as the last two rows in table (2).

plasma power		C1	C2.1	C3	C2.2	O1	O2.1	O2.2
0 W		0.26	0.18	0.19	0.00	0.19	0.19	0,00
1 W		0.29	0.16	0.17	0.00	0.19	0.17	0,01
2 W		0.28	0.16	0.18	0.00	0.19	0.18	0,01
4 W		0.30	0.16	0.17	0.00	0.19	0.17	0,00
6 W		0.33	0.15	0.17	0.00	0.18	0.17	0,01
8 W		0.36	0.14	0.15	0.00	0.17	0.15	0,02
10 W		0.34	0.14	0.17	0.00	0.18	0.17	0,00
12 W		0.35	0.14	0.16	0.00	0.17	0.16	0,01
15 W		0.33	0.14	0.17	0.00	0.18	0.17	0,01
18 W		0.32	0.16	0.17	0.00	0.17	0.17	0,01
21 W		0.37	0.14	0.15	0.01	0.16	0.15	0,02
25 W		0.35	0.15	0.16	0.00	0.18	0.15	0,01
30 W		0.39	0.13	0.14	0.02	0.15	0.14	0,02
35 W		0.39	0.14	0.14	0.03	0.16	0.14	0,02
40 W		0.39	0.13	0.14	0.02	0.16	0.14	0,02
50 W		0.46	0.10	0.12	0.05	0.12	0.12	0,03
65 W		0.43	0.11	0.14	0.04	0.13	0.14	0,02
80 W		0.49	0.10	0.11	0.04	0.11	0.11	0,03
100 W		0.58	0.10	0.07	0.03	0.08	0.07	0,05
120 W		0.53	0.09	0.09	0.05	0.10	0.09	0,04
linear fit	a	0.3	0.16	0.17	0	0.18	0.17	0
	1000 b	2.32	-0.64	-0.79	0.46	-0.91	-0.78	0.34

Table 3. *Chemical composition according to XPS result, the parameters of linear fit in form C(W)=a+b.W are shown in last two rows*

3.3.4 Nuclear Magnetic Resonance

The films prepared without plasma and at 2W, 10W, 30W, 100W of plasma power were

characterised by NMR. The bulk PLA polymer was also characterised by NMR for comparison. Hydrogen spectra were obtained for all the samples. The carbon ^{13}C spectrum, the Distortionless Enhancement by Polarization Transfer (DEPT) of carbon spectrum and also Heteronuclear Correlation through Multiple Quantum Coherence (HMQC) were obtained only for the sample at 10W of plasma power. By comparison of H ^{13}C, DEPT ^{13}C and HMQC spectra for 10W.it was possible to assign almost all of the observed peaks to carbons and hydrogens in different chemical groups. These spectra at 10W are shown in the figure (27). The assignment of 10W was used for quantitative analysis of other hydrogen spectra.

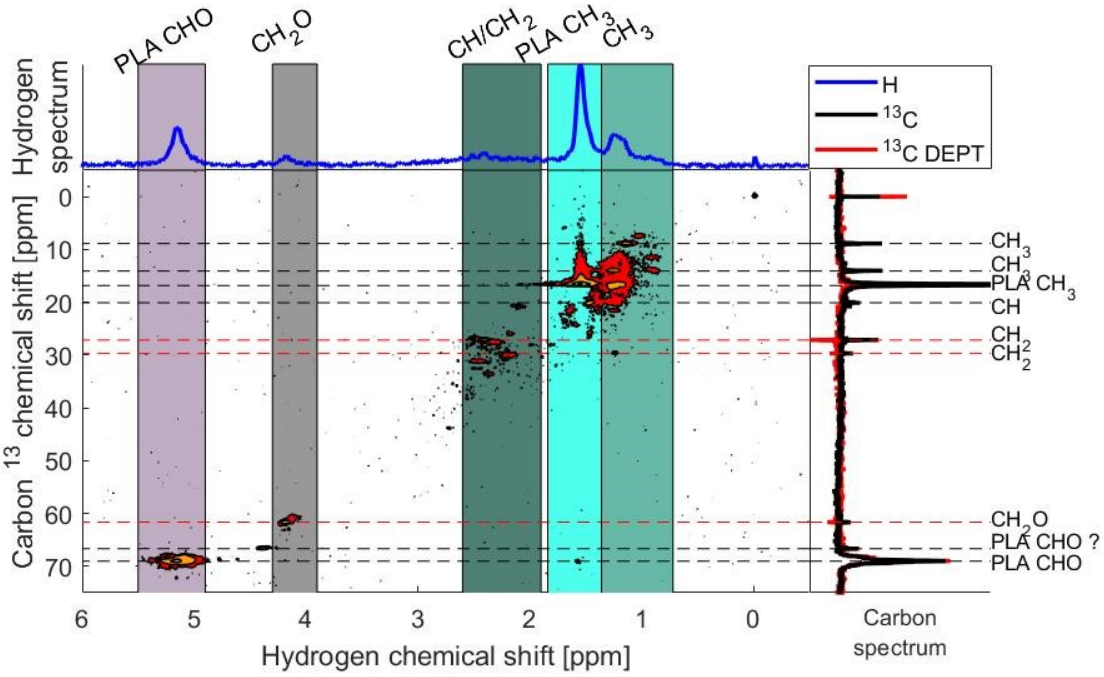

Figure 27. *NMR hydrogen (blue),carbon (black) , DEPT carbon (red) and HMQC spectra of sample prepared at 10 W of plasma power. The integration regions are distinguished by coloured rectangles*

The typical hydrogen NMR shifts for CH_x groups are from 0 up 2.5 ppm. This corresponds to our results, where several peaks were between 1.6 and 2.7 ppm, which were assigned to CH_x groups

Typically, CH_xO groups are between 3 and 5 ppm. In our spectra region there is a group of peaks from 3.9 to 5.5 ppm of chemical shift which matches the CH_xO chemical group. The hydrogen peaks at chemical shifts 1.5 ppm and 5.1 ppm in hydrogen spectra were assigned to CH_3 and CH in ester PLA groups. This assignment was based on the fact that

these two peaks were observed in all spectra from bulk to 100W of plasma power. We observed that the above peaks are in a ratio of 3:1, this matches to ratio of three hydrogen atoms bonded to aliphatic carbon in PLA and one hydrogen atom bonded to carbon in the polymeric backbone.

The region between 0.7 ppm and 1.4 ppm in hydrogen spectrum and from 9 ppm to 22 ppm in carbon spectrum was also assigned to CH_3, due to the relative proximity to CH_3 PLA peak.

There were no peaks in this region for lower plasma power, therefore, these CH_3 groups were not from original PLA.

The peaks at 27 ppm and 30 ppm in carbon spectrum produced a negative signal in DEPT ^{13}C spectrum. The DEPT spectrum is flipped for groups containing an even number of hydrogens. These peaks were assigned to carbons in CH_2 structure. Corresponding atoms in the hydrogen spectrum produce a chemical shift from 1.9 ppm up to 2.7 ppm. There is one more peak at 20 ppm of carbon spectrum, which we think is CH. Therefore, the whole region of 1.9 ppm-2.7 ppm of hydrogen spectrum was assigned to CH/CH_2

The peak between 3.9 ppm and 4.3 ppm in hydrogen spectrum was assigned to CH_2O groups, as it was in the region suitable for CH_xO groups and produced a negative DEPT signal.

There was one more peak at 4 ppm, which was clearly a CHO peak based on the proximity to other CH_xO peaks and positive DEPT signal.

There was one another peak at 140 ppm of carbon spectrum. This peak did not correlate to any hydrogen peaks, therefore, it indicates that it corresponds to carbon double bonded in PLA structure.

The above-mentioned intervals, which were shown in the graph as coloured rectangles in figure (27) were used as the integration limits for the quantitative analysis of the spectra at other plasma powers. The graph of all measured hydrogen spectra is shown below.(Figure (28))

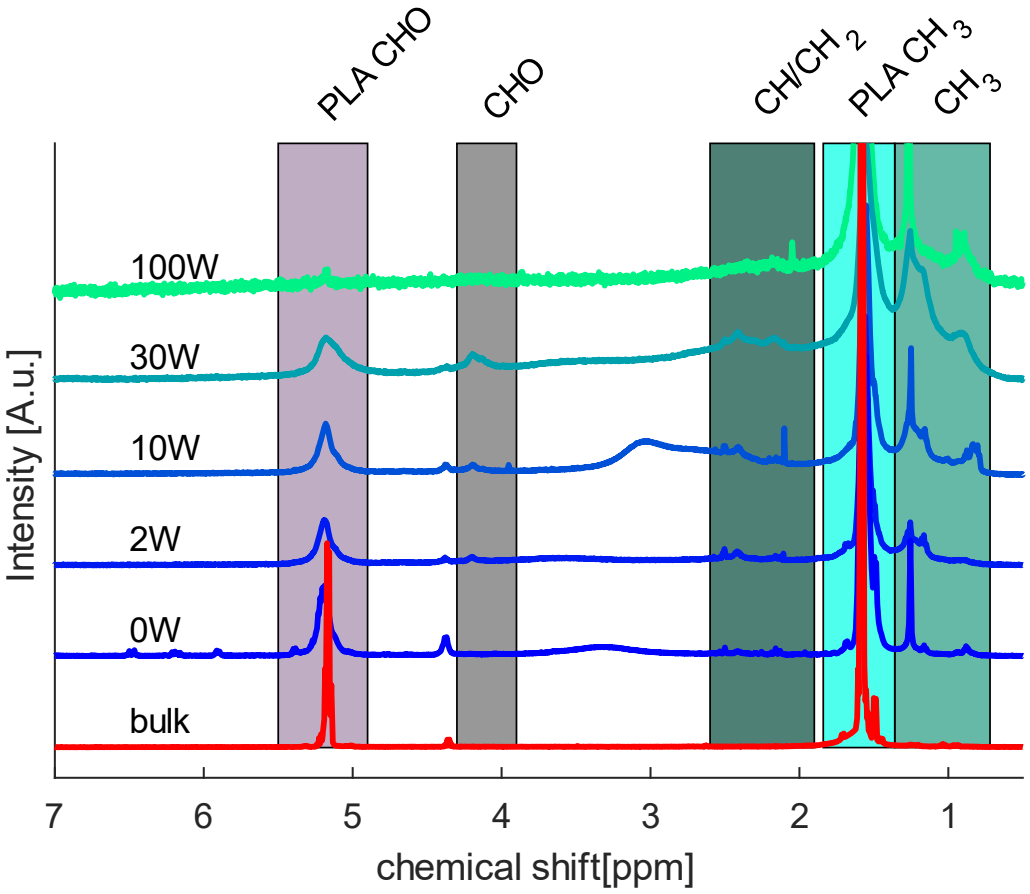

Figure 28. *NMR hydrogen spectra, The integration regions are distinguished by coloured rectangles*

The measured spectra were integrated in the regions discussed above. This gives us the relative contribution of hydrogens. The peaks were integrated and the relative areas of those peaks are shown below in table (3). The linear fit in the form

$$C(W) = a + b.W$$

for plasma power region 2-30 W is shown as two last rows of the table. The 100 W was not included into the fit because the integration of 100 W hydrogen NMR spectrum was very rough. The results are shown in figure (29)

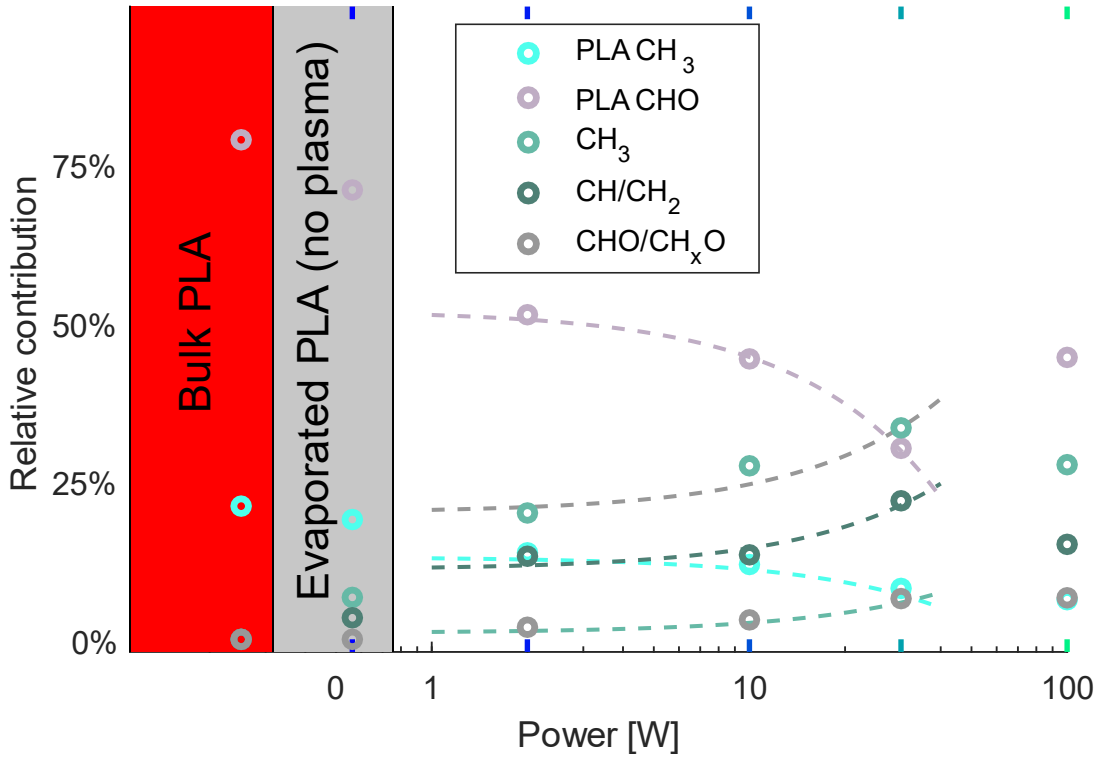

Figure 29. *Amount of Hydrogens in different chemical groups according to NMR*

plasma power		H in PLA CHO	H in CHO/CH_2O	H in CH/CH_2	H in PLA CH_3	H in CH_3
bulk		0.21	0.00	0.00	0.79	0,00
0 W		0.19	0.00	0.03	0.71	0,07
2 W		0.14	0.02	0.13	0.51	0,20
10 W		0.12	0.03	0.13	0.44	0,27
30 W		0.08	0.06	0.22	0.30	0,33
100 W		0.06	0.07	0.15	0.45	0,28
linear fit	a	0.13	0.01	0.11	0.52	0.20
	1000b	-2.00	1.60	3.40	-7.40	4.50

Table 4. *Amount of hydrogens in different chemical groups according to NMR, the parameters of linear fit in form C(W)=a+b.W are shown in last two rows*

This gives us the total contribution of all hydrogens in the films. However, for analysis and comparison with other results, it is beneficial to recalculate these results into the contribution of carbons. The integral for PLA CH_3 and CH_3 must be divided by a factor of 3. The CH_2/CH and CH_2O/CHO integrals (that not correspond to PLA CHO peak) must be divided by a factor in the range of 1 and 2. We observed from the graph that there are more CH_2(O) than CH(O) structures. For this reason we divide the CH2O/CHO and CH2/CH by factor 2. The last region has the same amount of the hydrogen as carbon and the factor is therefore one. The relative contribution of the carbon atoms in different chemical groups is shown below in the table (4).

Plasma power		C in PLA CHO	C in CHO/CH_2O	C in CH/CH_2	C in PLA CH_3	C in CH_3
bulk		0.44	0.00	0.00	0.56	0,00
0 W		0.41	0.00	0.04	0.51	0,05
2 W		0.30	0.02	0.15	0.38	0,15
10 W		0.27	0.03	0.15	0.34	0,21
30 W		0.19	0.07	0.25	0.23	0,26
100 W		0.15	0.08	0.18	0.36	0,22
linear fit	a	0,31	0.01	0.13	0.39	0.15
	1000b	-4,20	1.90	4.00	-5.30	3.60

Table 5. *Amount of carbons in different chemical groups calculated from hydrogen NMR spectra, the parameters of linear fit in form C(W)=a+b.W are shown in last two rows*

3.3.5 Comparison Between XPS and NMR Results

Both XPS and NRM provide us chemical information about the films. However, both techniques are sensitive to different elements, it is therefore not possible to simply compare the outcomes. However, if it is possible to make some assumptions about the structure of the material, the comparison can be done.

The XPS gives information that the layers are formed from original PLA ester groups, carbon rich chains and newly formed ether-like groups, fitted in XPS by PEG peaks.

Similarly, the NMR observed the presence of PLA ester groups, CH_xO ether groups and

additional CH_x aliphatic chains.

The mentioned structures are shown in the next figure(30) The XPS can distinguish between all different carbons and oxygens in these structures, but if an aliphatic carbon chain is formed in the structure the signal cannot be distinguished from PLA C1 carbon in XPS spectra.

On the other hand, NMR can distinguish between all hydrogens in all of these structures. It is possible to recalculate these hydrogens to carbons bonded to these hydrogens if the structure is given. The only structure, which NMR does not see is O-C=O in ester groups and oxygens in ether groups. These properties are shown in the next graph. The blue elements in the figure (30) below are invisible for respective technique.

	PLA	Aliphatic carbon chain (PP-like)	Ether (PEG-like)
XPS	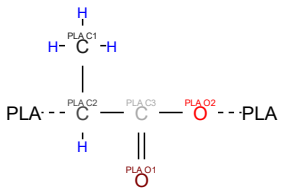	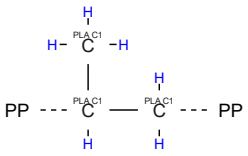	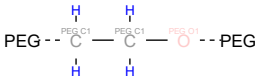
NMR	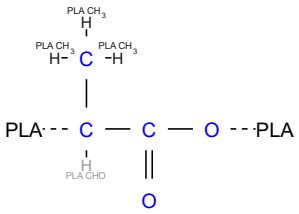	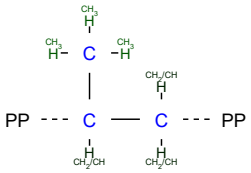	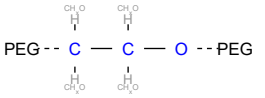

Figure 30. *Observable species with NMR or XPS in PLA-like, PEG-like, PP-like structure*

To be able to compare NMR and XPS results, we have to take the same subset of atoms, which are visible by both techniques. In PLA it is CH_3 group and CH in skeleton. These atoms are visible as PLA C1, PLA C2 in XPS and PLA CH_3, PLA CHO in NMR. From aliphatic carbon chain, all carbon atoms are visible in XPS as PLA C1 and in NMR as CH_3 and CH_2/CH. The carbons in ether groups are visible as PEG C1 in XPS and CH_xO in NMR. This is illustrated in figure (31), The red ones are elements, which are visible by both techniques. The yellow ones are visible either by NMR or by XPS but not with both.

	PLA	Aliphatic carbon chain (PP-like)	Ether (PEG-like)
	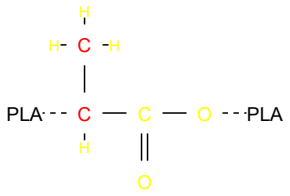	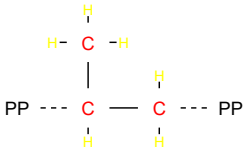	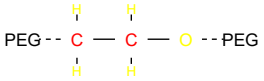

Figure 31. *Observable species with NMR and XPS in PLA-like, PEG-like, PP-like structure*

To visually compare the results we rearranged graph (26) into a cumulative form of graph (32). The components are stacked on each other. The total sum of the contribution equals one. We also added the theoretical bulk PLA and 0W as separate columns. The theoretical contribution of carbon in PLA C1 was calculated as an average of PLA C2 ,PLA C3 ,PLA O1 ,PLA O2 and was added as a white dashed line. The yellow points represent the measured values, not only from dataset E, but from all sets except dataset A.

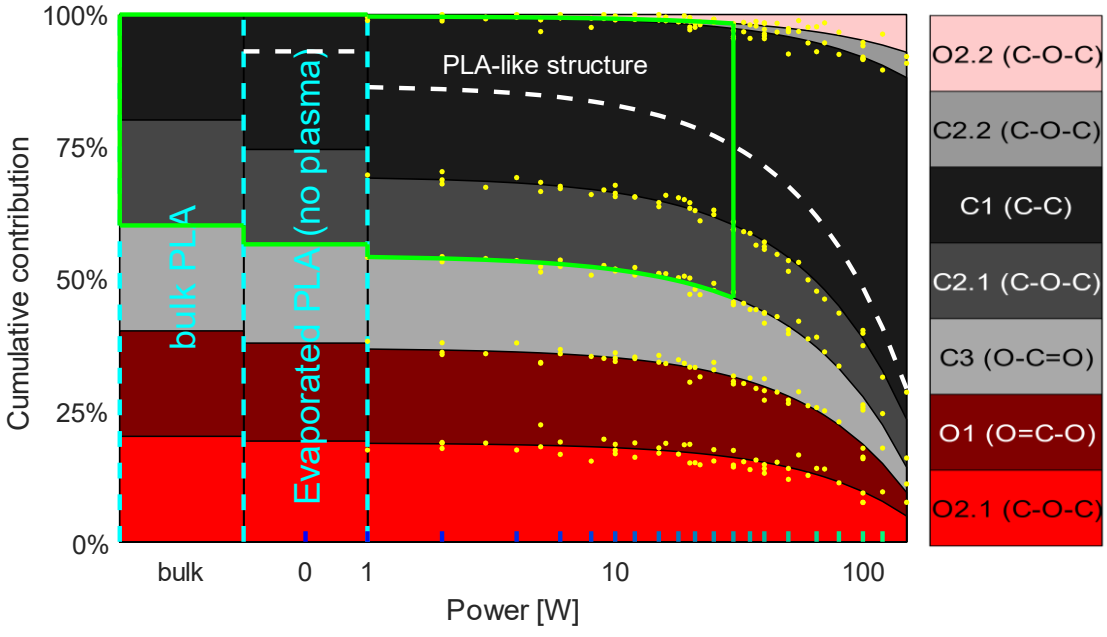

Figure 32*. Redrawn figure 26 into cumulative form. The green frame depicts a species which was possible to observe also with NMR.*

To be able to compare the NMR with XPS we have to take only the area within the the

green frame. This frame includes the PLA C1, PLA C2 and PEG C1 and corresponds to subset of atoms, which are visible also in NMR. The frame was rescaled to be rectangular shape and was plotted in the left side of graph (33). The similar NMR cumulative graph is shown on the right side.

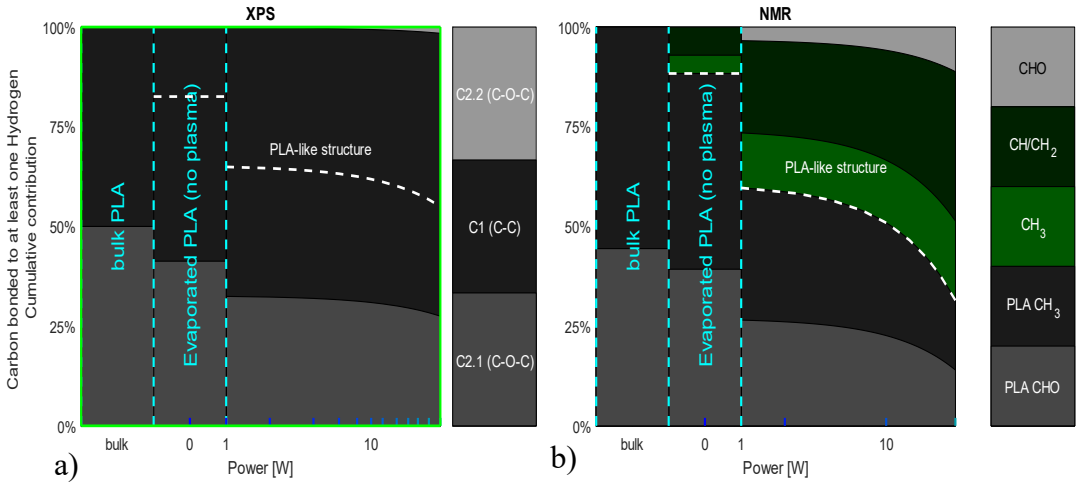

***Figure 33**. Comparison of XPS and NMR data. a) XPS, the green frame corresponds to green frame in the figure 32. b) NRM*

The XPS and NMR predict similar trends of decreasing the fraction of PLA with increasing power. The XPS shows slower chemical changes depending on the power than NMR. However, the results of both techniques are still in a very good agreement.

3.3.6 Gel Permeation Chromatography

The PAVTD phase initiates breaks of macromolecular chains. As result, the deposited coating consists of the polymeric chains shorter than original macromolecules. The sample prepared without plasma was not measured with GPC, because it was not possible to prepare enough material. The influence of plasma decreases the length of oligomers even more. On the other hand, these fragments are merged together in plasma. These lead to creation of a tail to larger molar mass in distribution This is demonstrated in figure (34), where molar mass of bulk PLA (red) and samples prepared with 2W, 10W, 30W, and 50W of plasma power are depicted. It has to be pointed out that the show results are from soluble part of the film. The unsolvable part of the film was filtered. Fraction of insolvable part was observed mainly for samples 30 W and 50 W of plasma power. This insolvable fraction is a densely crosslinked, therefore the molar mass of this fraction is much higher.

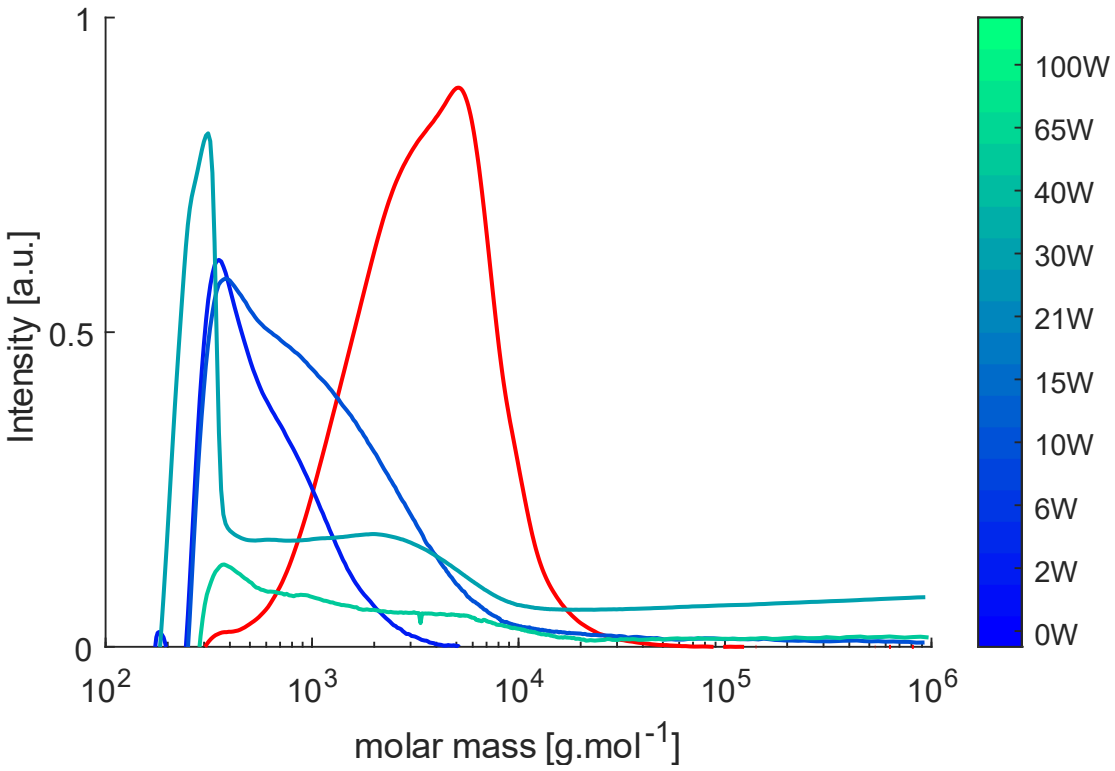

***Figure 34**. molar mass characteristics obtained by GPC, the bulk polymer depicted with red line*

3.3.7 Interpretation of Chemical Structure

The estimation of the stochiometric formula of plasma polymers is normally not possible. The classical plasma polymers are formed from small crosslinked fragments of original precursor. The final polymeric network is random, therefore, stochiometric formula does not exists for them.

For our films the situation is different. The hypothetical process in our case is firstly fragmentation, where the length of these fragments is in the range of several PLA units up to hundreds of repeating PLA units.

Secondly, these fragments are recombined. The middle of polymeric chains of those fragments is not modified and remains chemically unchanged. Only the end groups of these fragments are chemically modified. This process of fragmentation and recombination repeats again and again in plasma. Such kind of process leads to partly stochiometric and partly random structure as there are parts of original PLA and newly formed parts. The density of crosslinks, i.e. the length of fragmented chains, estimates the

ratio between stochiometric and random fraction.

Such hypothetical process can explain the trends, which were observed. The XPS data show that number of atoms in PLA structures decrease from 90% without plasma to 30% at 100 W of plasma power. This PLA fraction linearly drops when power is increasing. The fact that this process is linear is interesting and can mean that the density of crosslinks depends on the power of plasma by some simple function.

The one part of newly formed structure consists of ether groups, which can be created by release of C=O from original structure. This leads to formation of C-O* radical, which can be recombined with another fragment of PLA and form an ether group. The second part of newly formed structure is formed by carbon rich polymer. This component is also formed from original PLA, because no other substance is included in the process. That basically means that all of the oxygen is released from the original PLA structure, which creates this carbon rich part. We think, that this is possible by releasing CO_2.

To support this model, we developed a simple chemical model, which describes this kind of reaction.

The one unit of PLA can be fragmented on five places. These positions of fragmentation are shown on figure (35)

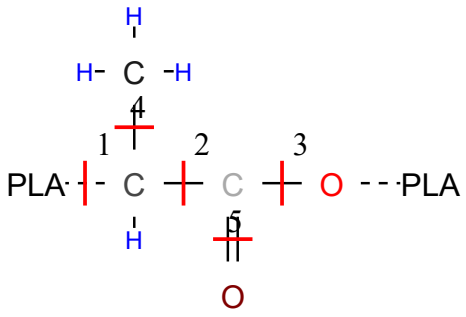

***Figure 35**. Possible places, where PLA can be fragmented*

, where positions 1, 2 and 3 are on the skeleton of the polymer and 4 and 5 are side groups. Let us assume that the PLA is not fragmented at positions four and five. This is probably not true, however, to keep the model simple we will not allow to create the branched structures. Also, the structures which has replaced aliphatic PLA C1 atom or double bound oxygen PLA O1 by single bound oxygen atom are ruled out by XPS data. This is caused by the fact that carbon in the O-C-O structure has binding energy of 288 eV. This

energy is exactly between PLA C2 and PLA C3 XPS peaks, where the minimum in our results is placed. Therefore, this structure cannot be created statistically significantly. If the single bound carbon would be bound instead of doubly bound oxygen, the structure would not be very different from the ones described below.

If the PLA is fragmented at positions 1 or 2then one of the fragments has O=C*-O or O=C-O* end group. This is depicted at figure [36] at row 1 column 1 and 2. If the PLA is fragmented at position 3 the C*=O is an end group of one of fragments. We think that these bonds can be released in the form of CO_2 and CO. Such kind of release of carbon oxides from polymers in plasma has been published in [33]. This is a way how the oxygen can be released from the structure with increasing number of fragmentations.

In this way the radicals O-*C-CH_3 and *O-C are formed. This is depicted on figure (36) at row 2. These radicals, which do not have to be product of one fragmentation, merge together forming final structure. Product of these recombinations are shown in row 3. There we assume, that the hydrogen can change the position and became radical -CH_2-CH_2*, which existence NMR predicts instead of -*C-CH_3.

		Column 1 (process 1)	Column 2 (process 2)	Column 3 (process 3)
Row 1	Fragmentation	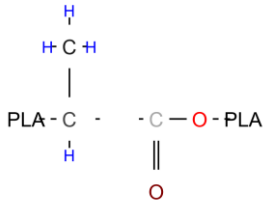 Fragmentation at pos. 1	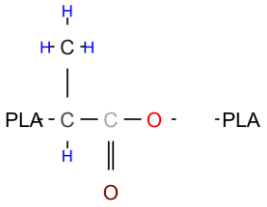 Fragmentation at pos. 2	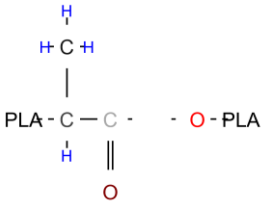 Fragmentation at pos. 3
Row 2	Release of end group	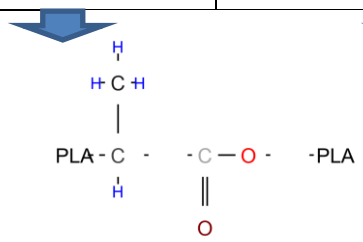 Release of CO2		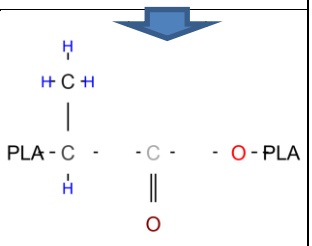 Release of CO
Row 3	Recombination	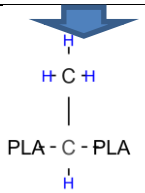 Product 1	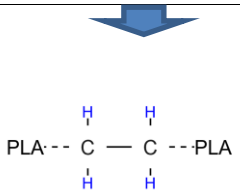 Product 2	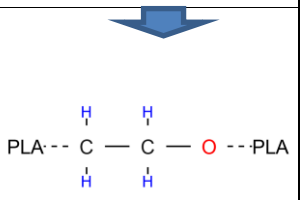 Product 3

***Figure 36**. Chemical model of repolymerization of PLA in plasma*

By this chemical model we can simulate XPS results. It is possible to calculate how the amount of atoms changes from XPS point of view. On the CO_2 release path one PLA C3, PLA O1 and PLA O2 atom is lost. The PLA C2 is transformed into aliphatic PLA C1 atom. Similarly, CO release path can be estimated. This is shown in table (5).

	PLA C1	PLA C2.1	PLA C3	PLA O1	PLA O2.1	et. C2.2	et. O2.2
Before process	a	b	c	d	e	f	g
After one process 1	a+1	b-1	c-1	d-1	e-1	f	g
After one process 2	a+1	b-1	c-1	d-1	e-1	f	g
After one process 3	a+1	b-1	c-1	d-1	e-1	f+1	g+1

***Table 6**. Change of structure with one reaction accordiong to chemical model depicted in figure 36*

, where a, b, c, d, e are number of atoms in particular group. In ideal infinite PLA chain a = b = c = d = e = n, where n is number of monomeric units and f = g = 0. The result of process 1 and 2 is the same. As an initial assumption the rate of process 3 was set as ten times lower than process 1 plus 2. The processes 1 and 2 and 3were repeatedly applied on the molecule of ‘’infite’’ length (n = 1 000 000) with their respective rates. Potential fragmentation of already modified units was neglected. In dependence on the number of repeating reactions the chemical composition according to XPS was calculated. The results of XPS simulated composition are shown in figure (37). As the dependency on the ratio of undisturbed PLA units to the units that underwent some of the fragmentation process. This ratio is also rough indicator of mean length of undisturbed PLA chains.

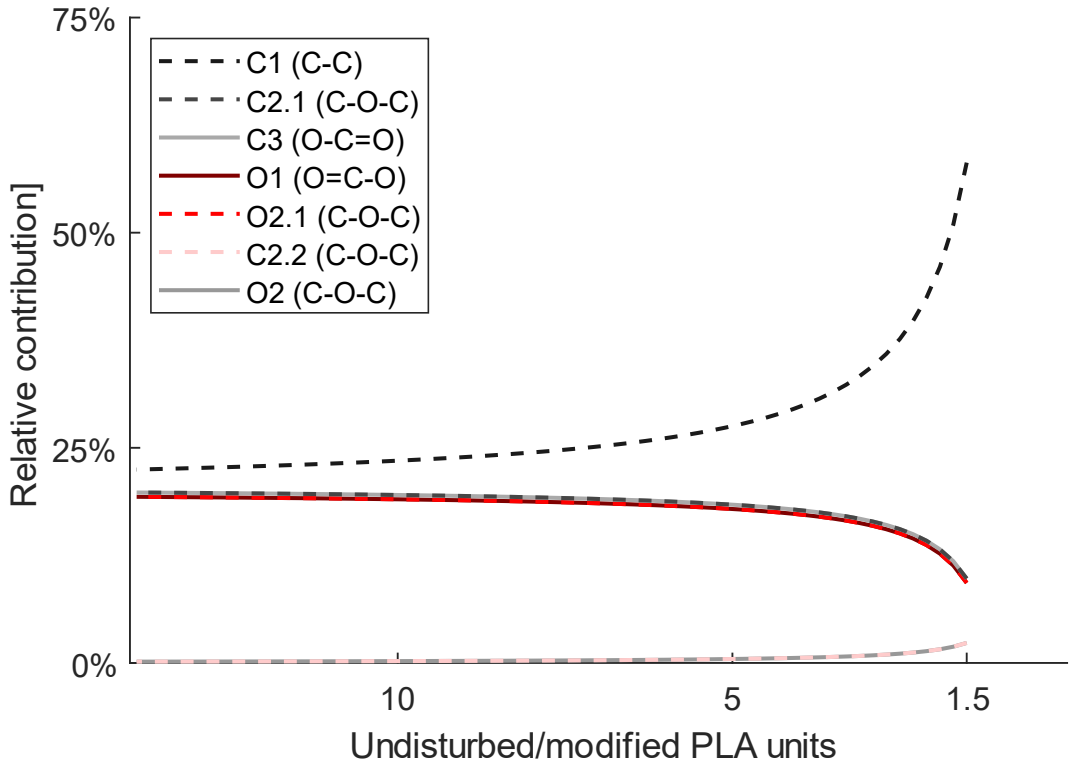

Figure 37. *Chemical composition calculated with model, in dependence on lenght of undistrubed/modified PLA units*

The shown interval of PLA fraction is similar to the interval measured with XPS varying from 90 % without plasma to 30 % at high plasma powers The mean length of nonfragmented parts is from 1 up to 10 repeating units of PLA units in this model. This does not have to be correct, because the carbon rich fragments can be formed by longer sequence of carbon atoms. Then the length of PLA parts can be longer.

If we assume that any of the previously mentioned fragmentation process take roughly same amount of energy, then the relative amount of energy required for creation of the structure with given chemical composition can be calculated.

$$C(power) = C(l_0).\Delta E\,\frac{l}{l_0} \qquad 8)$$

where C(power) is relative chemical contribution depending on power, $C(l_0)$ is relative

chemical contribution depending on the length of fragments-which is figure (38), ΔE is energy of one reaction, which is not known. However, ΔE is just a scaling factor, l is length of original PLA, again a scaling factor and l_0 is length of fragments.

The figure (37) can be recalculated depending on the relative energy deposited into original PLA and it is shown as figure (38) in the left side. In the right side is shown for comparison the original XPS results.

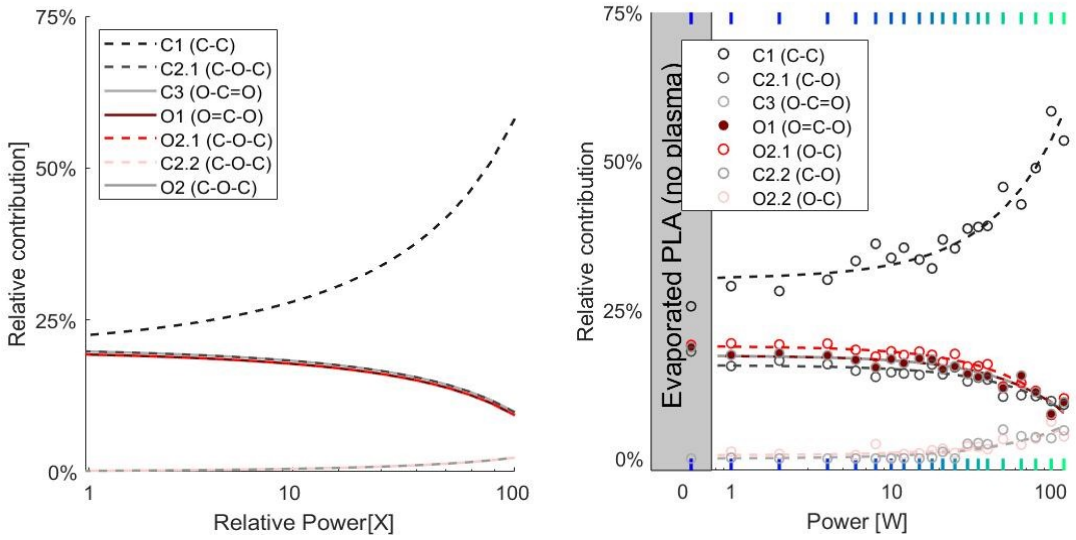

Figure 38. *Comparison of model and results obtained by XPS. Left: Chemical contribution calculated with model, in dependence on relative power. Right: Chemical contribution by XPS (Same as figure 26.)*

This model is oversimplified. The assumptions shown in table (5), figure (35) and equation (8) cannot be fully true. However, the main aim of this part is to show that the film is probably formed by original PLA chains connected together by carbon rich parts. Creation of ether groups can be natural process of fragmentation of PLA. The linear dependence of chemical composition depending on plasma power can be explanation just in simple quantitative scaling of frequency of fragmentation processes with a plasma power, without the necessity to consider qualitatively new fragmentation processes.

3.4 Macroscopic Properties of PAVTD PLA Layers

The main application potential for this kind of plasma polymer films is a barrier layer for drug delivery systems. The applications require to control the rate of release of the drugs from carrier material. This release rate can be modified by adding barrier layer which is dissolved in time and releases the drugs. For this reason we were mainly interested in the properties of films in water like hydrolysis, solubility and permeation through the layers. The water contact angle and ellipsometry were done on set D. It is the same set used for FTIR and XPS chemical analysis. Separate sets C and H were prepared for hydrolysis and permeation.

3.4.1 Water Contact Angle

The static water contact angle for all layers prepared at different plasma powers exhibits hydrophilic behaviour. The films prepared at up to 15 W of plasma power have high affinity to water with water contact angle between 10°-25°. In the region of 15-35 W of plasma power the water contact angle is rising up to 60°. Above 35 W the contact angle seems to be almost constant. This trend is in agreement with the chemistry results. The films prepared at higher plasma powers have less polar oxygen groups, which leads to lower surface energy and lower water contact angle. However, the chemical results of XPS and NRM exhibit more linear dependency on plasma power than WCA.(Figure (38))

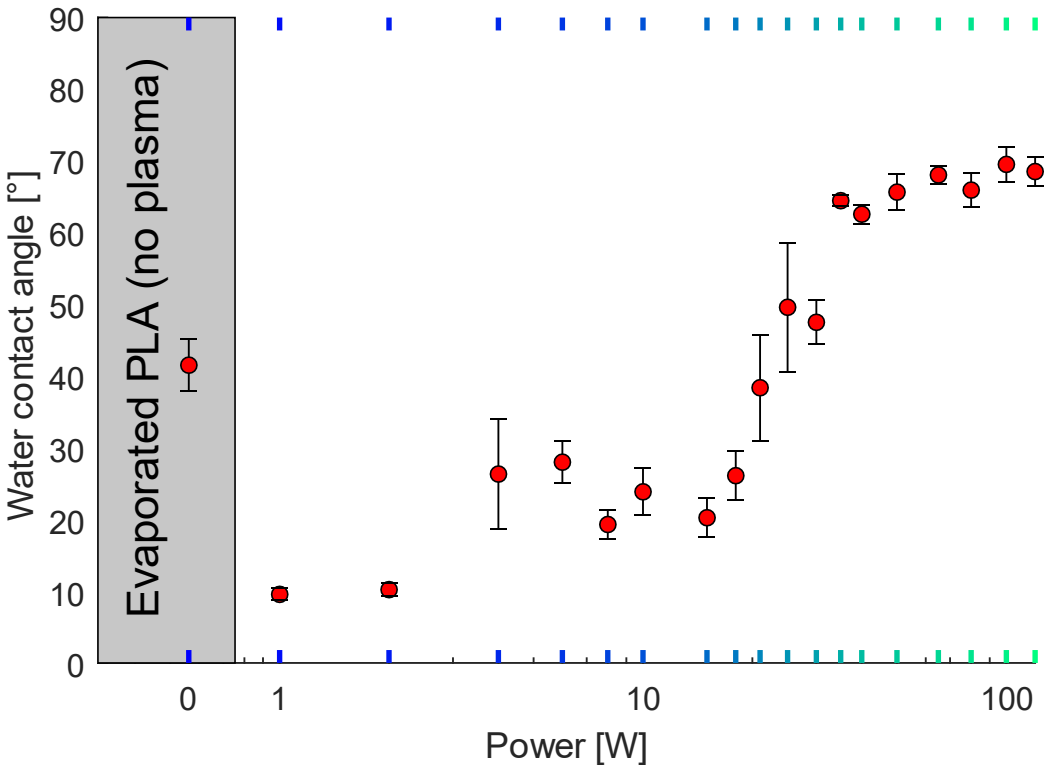

***Figure 39**. WCA measurements*

3.4.2 Ellipsometry – Thickness and Optical Constants

The dissolving of films in water was characterised by spectroscopic ellipsometry.

The graph of original thicknesses, before immersion in water of set D is shown in figure (39). This set was used for ex-situ and in-situ degradation tests. The other sets C and H used for hydrolysis and permeation had similar distribution of thicknesses and mean thickness as the D set.

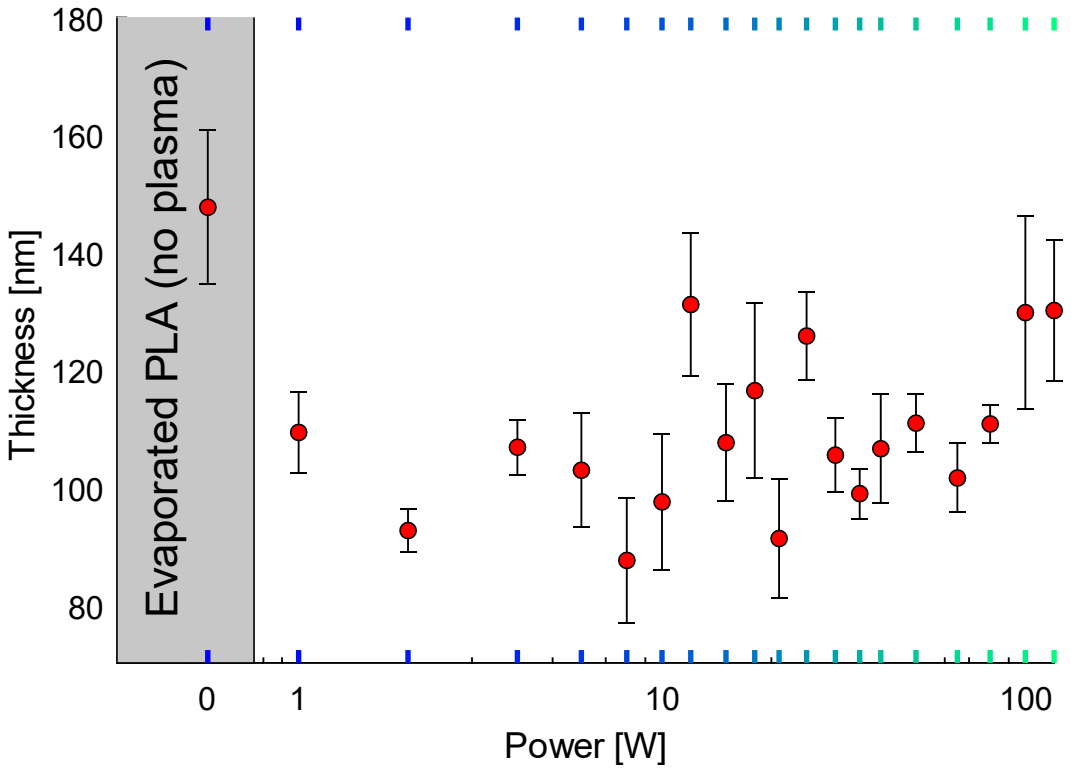

***Figure 40**. Thickness of films after deposition measured with Ellipsometry*

The amount of deposited material was controlled in-situ during deposition with QCM crystal. The change of frequency of QCM was kept constant for deposition of each sample, therefore, the amount of deposited material on the crystal during the deposition should have been constant. The thicknesses of films measured after deposition with ellipsometry varied in range from 80 nm to 150nm. This could be caused by different position of QCM and substrate holder. However, we assume that the distribution of the thicknesses is narrow enough, not to influence other measured properties like solvation and permeation of the films.

To be able to obtain thicknesses of films, the optical model has to be created. The Cauchy model was used for fitting of these films. The fitted parameters are thickness and optical constants. The fitted optical constants n and k are shown in figure (40). The n and k are functions of the wavelength, but for simplicity only n and k for 589 nm wavelength are shown.

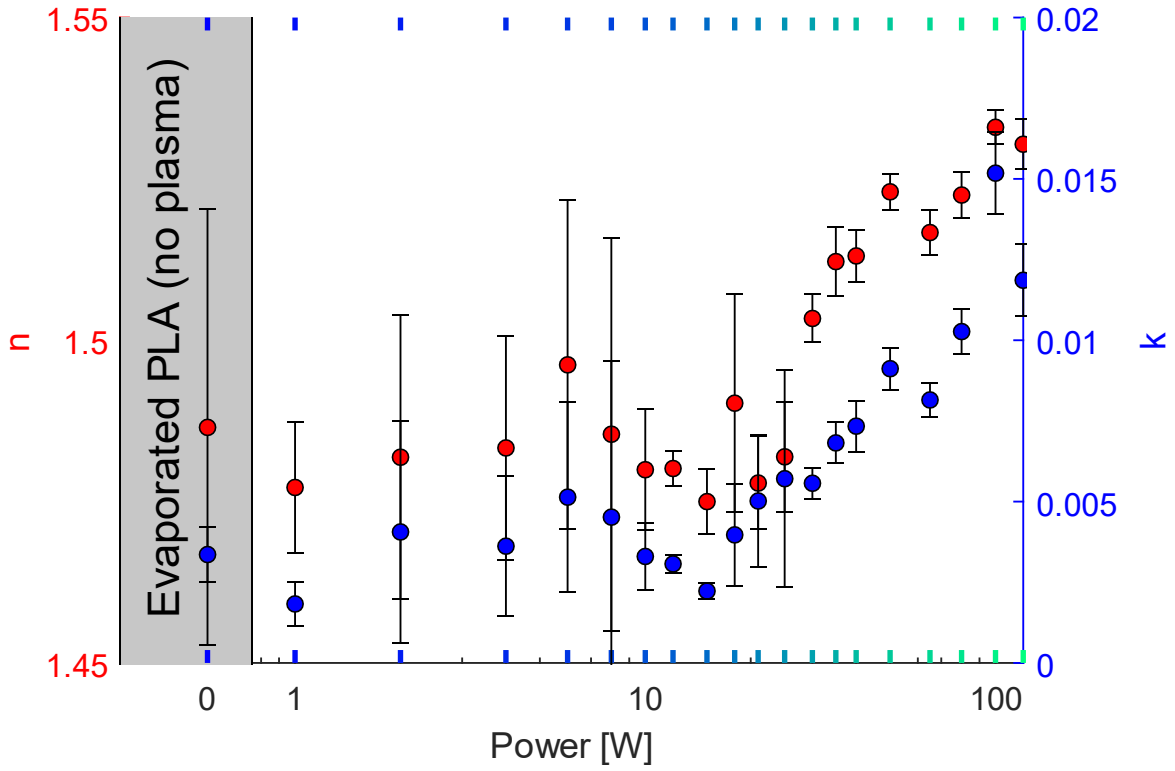

***Figure 41**. Optical constants of films after deposition measured with Ellipsometry*

The similar trend as was measured for water contact angle appeared in n and k data. Under 30 W the n and k are constant and above 30 W are rising. It is well known that there is a correlation between increase of CH polymers and increase of refractive index n [34]

3.4.3 Ellipsometry – Ex-situ Study of Films Degradation in Water

A set of 10 samples was prepared for all plasma powers. The thickness of all samples was estimated on three spots on each sample and these samples were then immersed in water. The set of samples was taken out of water at the times 1, 5, 15 seconds, 1,5,30 minutes, 2, 8,24 and finally 168 hours. The samples, which were in water more than 5 minutes were then let dry in open air. The samples immersed less than 5 minutes were gently dried with air flow. The thickness of these samples was then measured at three spots. The ratios of thickness before immersion and after immersion were calculated and are plotted in the 2d map (figure (41)). The inset shows in detail this ratio for 15 seconds and 1 day. The X axis in the inset is plotted linearly, to highlight the changes around 30W. The white points in the main graph represent the points, for which the SEM images were obtained after drying.

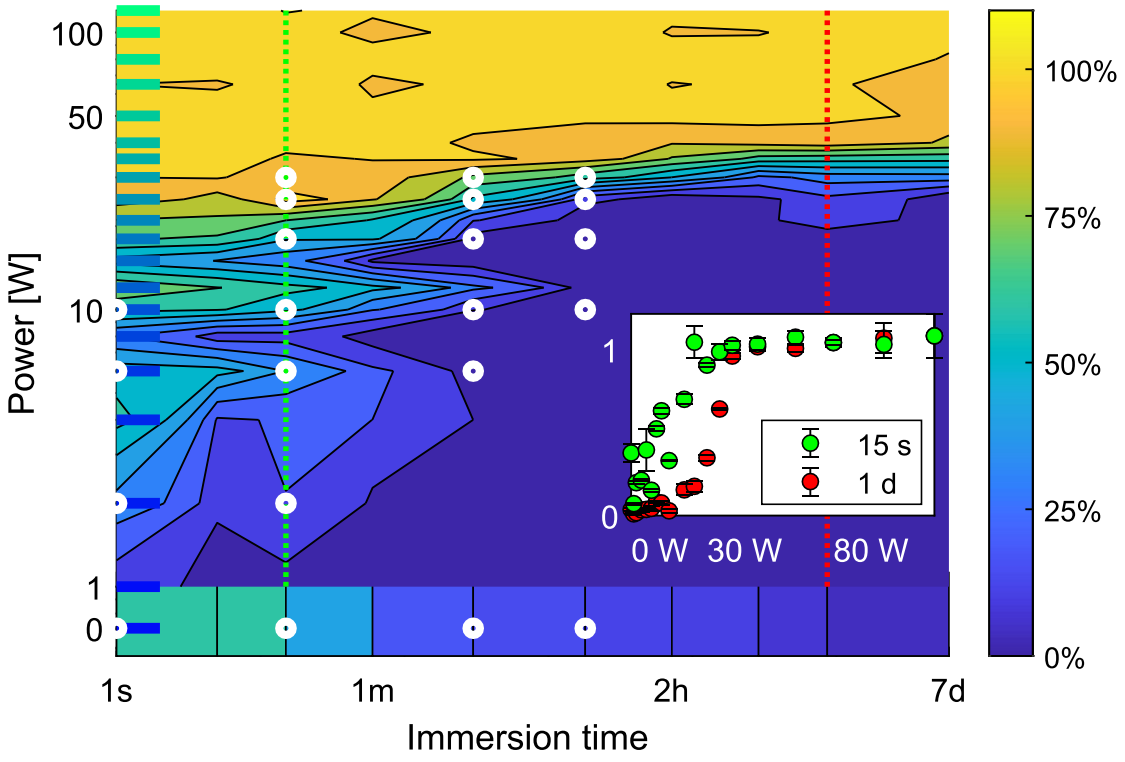

***Figure 42**. Graph of thicknesses after/before immersion. The ratio of thickness after and before immersion is depicted in colour gradient. The inset show this ratio for 15 seconds and 1 day. The white points shows, where SEM images were obtained.*

The films prepared with power of 1 W - 25 W degrade in water in a time range of 30 minutes. The degradation rate of these samples depends on the plasma power. The samples prepared at the lowest power dissolve most quickly and this degradation rate is slowed down with increasing power. This can be explained by an increasing number of crosslinks in the structure and transition between sol and gel type of the structure. At power above 40 W the layers do not seem to dissolve in water over the range of one week. Probably there are so many crosslinks in the structure, that the structure does not degrade. There is a sharp transition between these two regions in the range from 25 W to 40 W of plasma power. We do not have clear explanation why there is such a sharp change around 30W, while the chemical composition behaves linearly with the power. However, it can be observed that also other properties like a water contact angle, optical constant and other changes are also in this region.

The sample prepared without dissolves in similar time as samples prepared at 10-20W.

This is in good agreement with water contact angle analysis, where the samples without plasma has similar WCA as the samples 10-20W.

To study the structure of the immersed layers, the SEM images were obtained after the drying of the films. The images are shown in figure (42). The scale of shown SEM images is 10 μm in both directions. The SEM images in blank positions in the table were not obtained, because of impossibility to focus on anything on these samples.

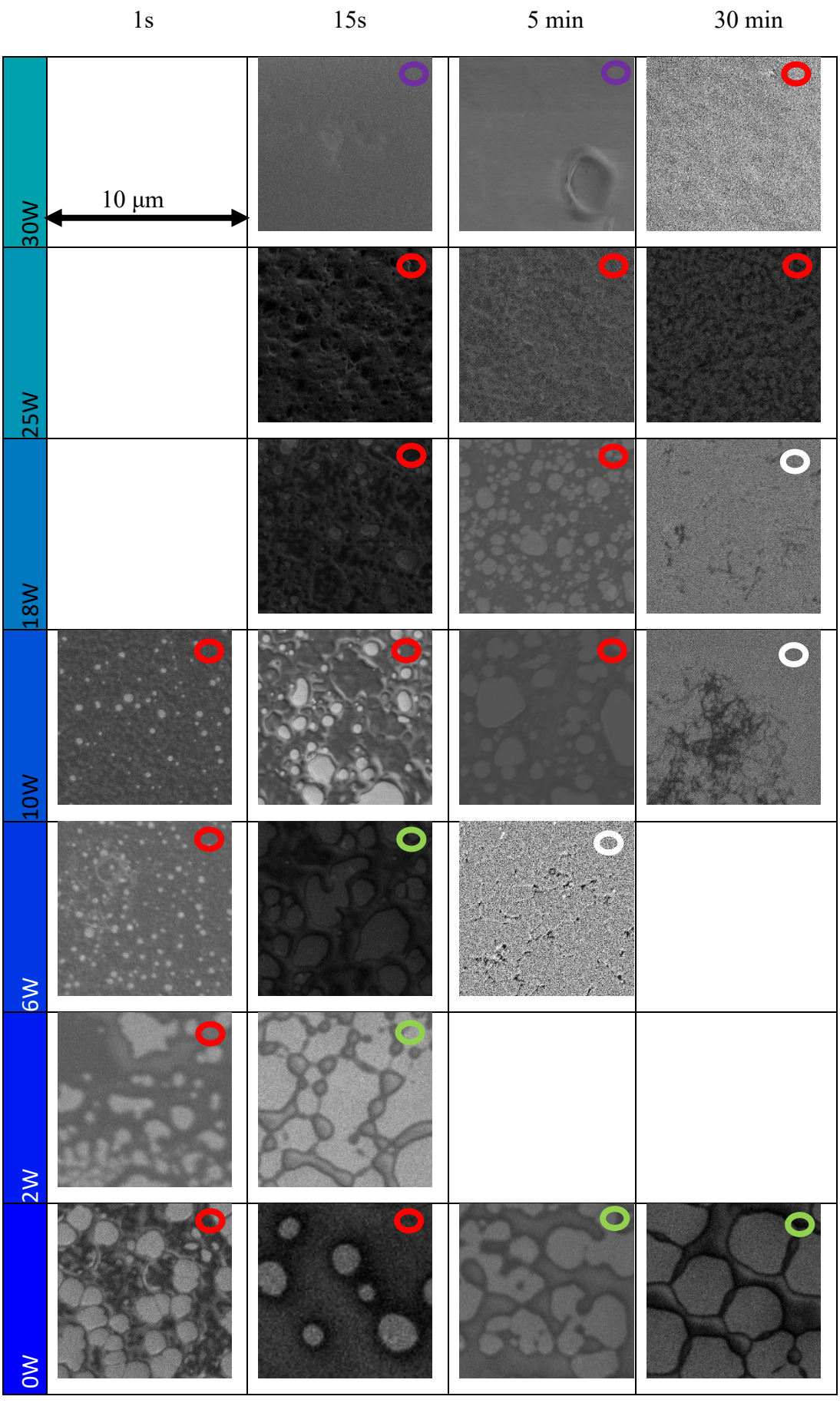
1s
15s
5 min
30 min
30W
25W
18W
10W
6W
2W
0W
10 µm

***Figure 43**. SEM images obtained after immersion. The scale of the images is 10 µm in both directions. The circles distinguish between different types of structures: red-holes in strucutre, green- connected spots , white – almost dissolved structure, purple – blister structure*

The similar development of the structures was observed for all of the plasma power up to 30 W, but the timescale of the changes depends on the plasma power. The process was subjectively divided into several steps. These groups can be distinguished by different coloured circles in the top right corners. In the first step – red circles, there are holes, or some inhomogeneity in the structure. The process of dissolution continues till just some spots connected together by thin linkers remain in the structure. This step is marked by green circles. At the end only some small remnants of these structures remain, which is depicted by white circles. The degradation of films prepared at higher plasma looks differently. There were observed some blister like structures as depicted by purple circles.

3.4.4 Ellipsometry – In-situ Study of Films Degradation in Water

The above mentioned ellipsometry and SEM experiments gave us information about the structure of films after drying. However, the most interesting processes of decomposition and swelling occur during the immersion. To study these processes in-situ we employed the water-filled liquid ellipsometric cell. The samples were immersed for 12 hours. The graph of thickness after/before immersion (cf. figure (41))is shown below again with added regions as red lines, where in-situ experiment was done (figure (43)).

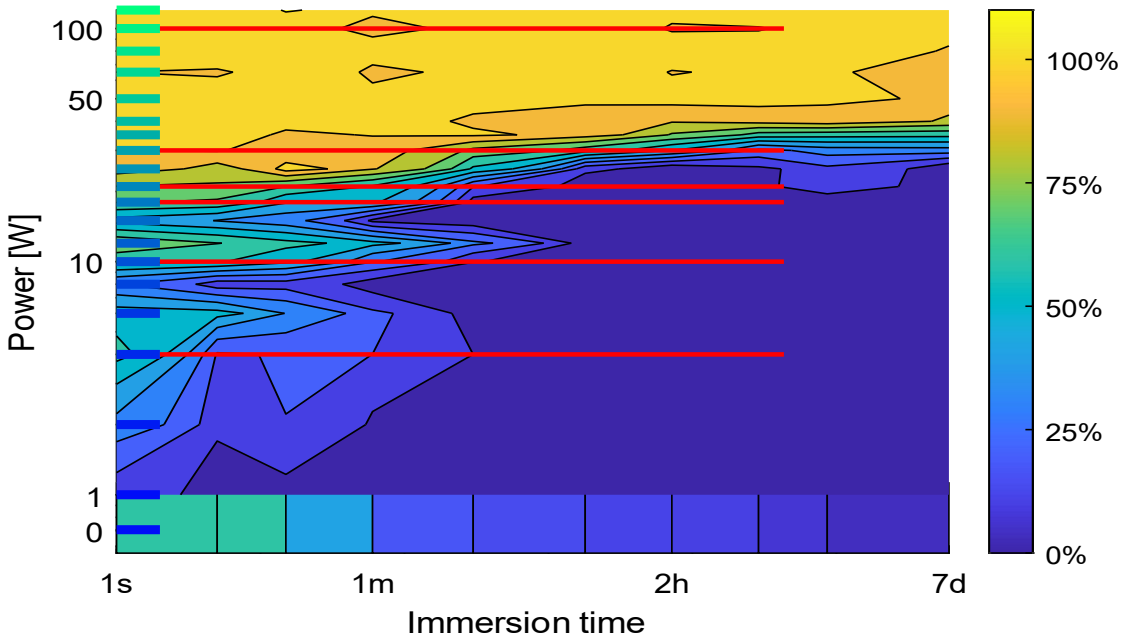

***Figure 44**. Figure 41 of thicknesses after/before immersion reprinted with added regions (red lines), where in-situ ellipsometry was done*

We were not able to analyse the rest of the samples from the set. It can be seen that the above shown data from thickness after/before ratio are not ideal. For example, samples prepared under 8 W and 15 W of plasma power do not match the trend. The similar irregularity was even higher in in-situ data. This was caused by nontrivial properties of the films. It was found that these films did not behave like solid films in water, especially, the ones prepared with weaker plasma power up to 30 W. These films were able to absorb so much water, that the optical indices were almost same as for water. This caused an issue for ellipsometry analysis, because the fit was unstable.

To be able to compare the results from ellipsometry it is necessary to fit all the data with one model. This is not simple, because samples prepared with higher plasma power do not absorb any water and have totally different properties comparing to the samples prepared at lower power. For above mentioned reasons it was necessary to keep the number of free fitting variables as low as possible and make the model physically intuitive. The free parameters of the final model were the overall thickness and the ratio of water compound in the films, whereas the effective medium approximation optical model was employed. The optical properties of the films in the form of Cauchy model were taken from the fit before immersion. We assume that the optical properties of the

film do not change in water. The film with these optical properties was taken as one medium of effective medium approximation model. The second medium was water. The results are shown in figure (44).The thickness in time is shown on the vertical axis. The ratio of water in film is shown as the colour. The films consisting mostly of water are depicted by dark blue colour. On the other hand, films which did not absorb any water are shown in yellow colour. The empty space depicts time for which the model did not predict physical results.

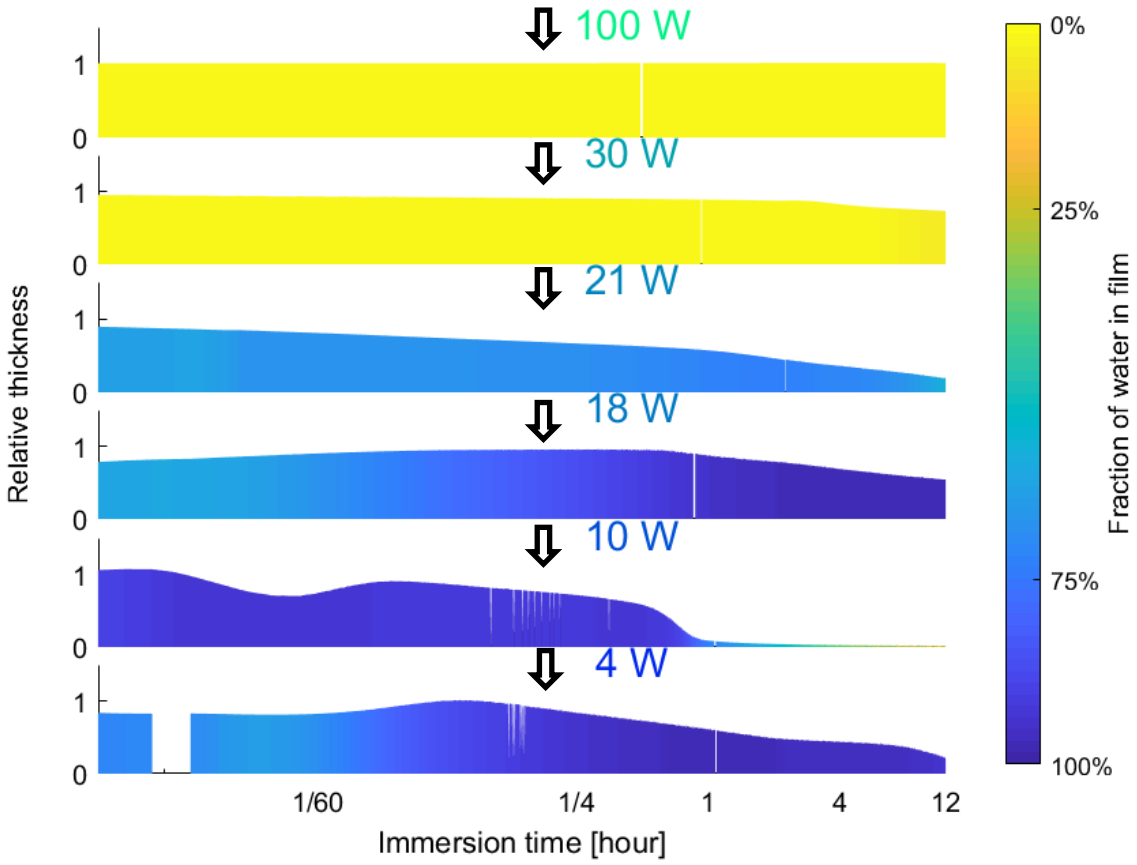

***Figure 45**. In-situ swelling of the films measured by ellipsometry with samples in liquid cell. The thickness in time is depicted on the y axis of the graphs, the amount of water is depicted as colour gradient. Dark blue correspond to water, yellow to solid film.*

The changes appearing around 20 W - 30 W of plasma power, where sharp transition between dissolvable and unsolvable behaviour occurs in previous results, were visible also for in-situ swelling. It can be seen absorption of water for lower plasma powers. With increasing power the films are absorbing water slower. The interesting fact can be

observed after comparison with the graph of thickness after/before immersion (cf. figure (41)). The ex-situ analysis predicted that after several minutes of immersion the films were almost washed off in samples prepared with lower plasma powers. The in-situ results said that some fraction of the films was still present, however, these residues were completely swollen. These swollen residues were probably washed off by process of taking samples out of water and drying. Therefore, they cannot be observed after drying.

3.4.5 Hydrolysis

The hydrolysis characterisation was done at Tomas Bata University in Zlín. The reaction of PLA with water was studied. The PLA chain is decomposed into one-unit shorter PLA chain and lactic acid monomer. The chemical equation of this reaction is depicted in figure (45)

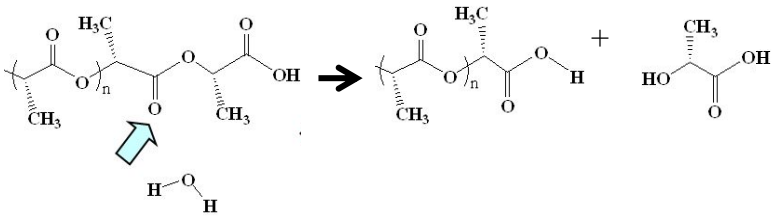

***Figure 46**. Hydrolysis reaction of PLA*

The hydrolysis of the films was studied on the set C. Therefore, the results can vary slightly from previously mentioned experiments, which were done on other sets.

First concentration of LA monomer was estimated in 2 hours after immersion. The next ones were taken at four, six and seven days. The data are depicted in figure (45). The points 2W 30W and 40W at seven days were not taken. The powers above 50 W of plasma power were not obtained.

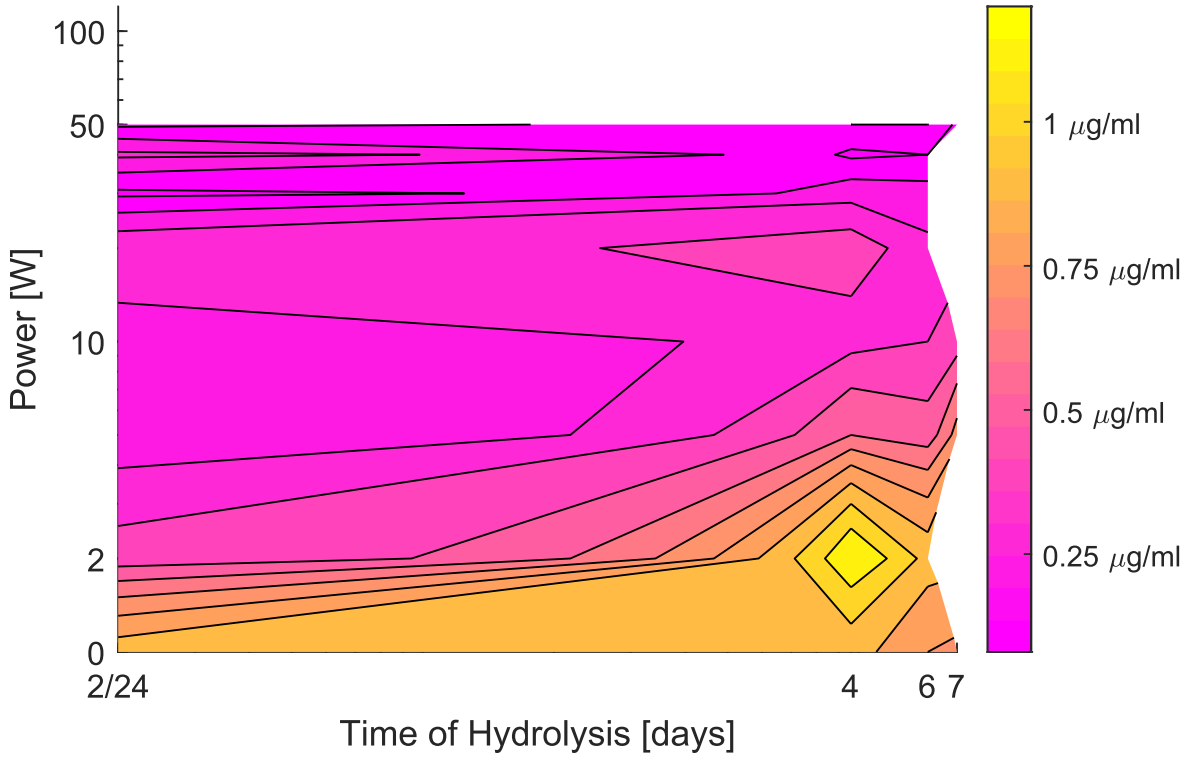

***Figure 47**. Graph of hydrolysis.The estimated concencration is shown with gradient of colour, where purple no LA, yellow most LA*

The highest concentrations were observed in time scale of several days. This is in good agreement with the fact, that this is a chemical reaction, which is slower that the physical dissolving characterised above with ellipsometry. The most of lactic acid was released from samples prepared by lowest plasma power. This is a logical result, because from chemistry part of this research we know that the films prepared in weakest plasma consisted mostly from PLA and their chains were the shortest having many end groups where the reaction can occur.

There was one more trend in hydrolysis data: the decrease of lactic concentration above 30 W of plasma power for all time of measurements. This was possibly the same effect as was shown on previous immersion graphs, where the samples above 30 W of plasma power were not dissolving in the water, therefore, the hydrolysis can not occur for these samples.

3.4.6 Permeation

The main application potential of such kind of films is barrier layer. Therefore, one of the most interesting characteristics is permeation through the layers of active species. Several model molecules of different molar mass were tested to get the permeation behaviour of our layers. The molecules with higher molar mass are bigger, therefore it can be expected that these bigger molecules permeate through the barrier layers slower The sodium salicylate(160 g/mol) (SS), cetyl pyridinium bromide (380 g/mol) (CPB), nisin (3300 g/mol) and bovine serum albumin (66430 g/mol)(BSA) were employed to study the permeation through the films. Only the results for Nisin and CPB are shown in this thesis. The results for other molecules did not have been properly analysed yet.

The active molecules-containing layers were prepared via spin coating on the silicon substrate. Subsequently, PLA-like PAVTD polymer layer was deposited on the substrates.

The samples containing the layer of active sample and PLA thin film were immersed in water At defined time intervals, 1 ml was withdrawn for analyses. The time, when the samples were taken out of water were 3, 8, 30 minutes, 2, 4, 8 hours, 1, 3 days and finally one week. The permeation tests were done up to 100 W. The different dataset from the set used for ellipsometric immersion analysis were used. The results for permeation of nisin are shown in figure (46).

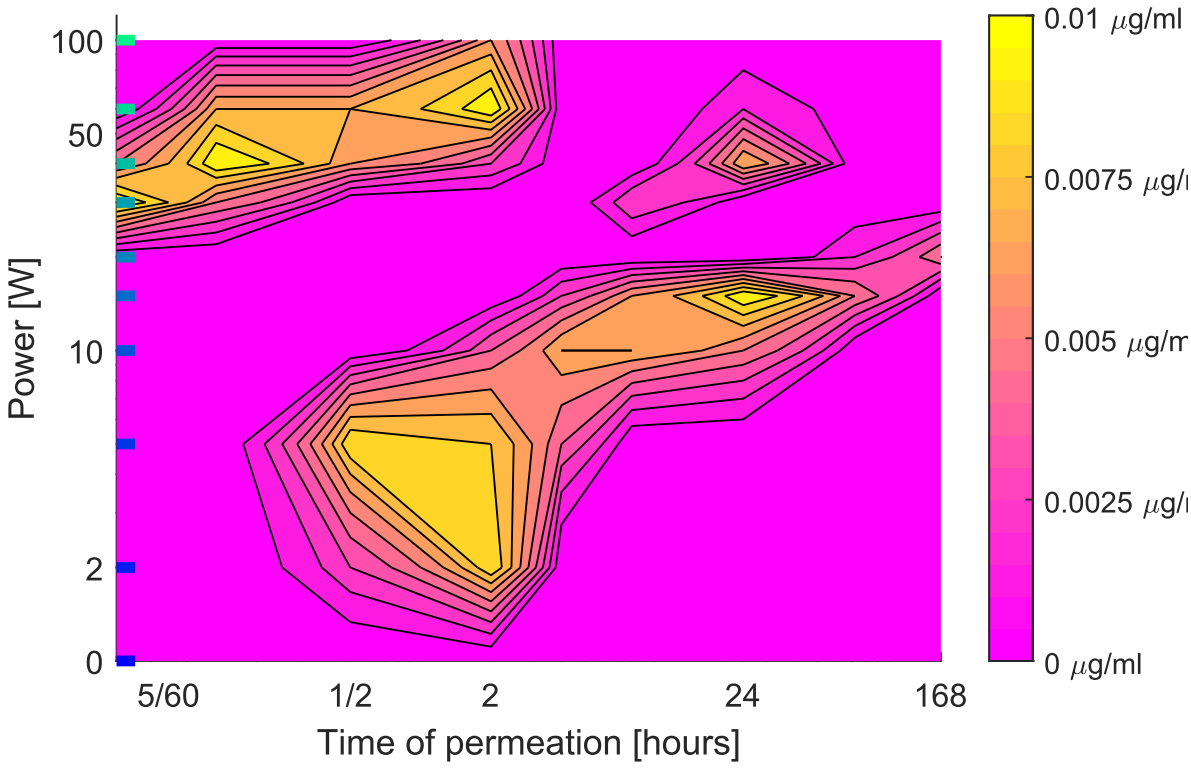

***Figure 48**. Graph of Nisin permeation through the films The estimated concencration is shown with gradient of colour, where purple no Nisin, yellow most Nisin*

The nontrivial behaviour of nisin permeation through the films was found.

Firstly, the expected result of permeation below 30 W of plasma power was observed, where the time scale of permeation depends on the power. The films prepared at higher power exhibits slower permeation. This can be expected as the films prepared at higher plasma power shall be more densely crosslinked than the films prepared with lower powers.

Secondly, the region above 30W of plasma power is surprising. It seems that the Nisin permeates through the films prepared with plasma power above 30W quicker than through the films prepared in weaker plasma. This is strange, because we expected that the permeation will be much slower. It has to be pointed out, that this change in behaviour happens at 30 W of plasma power, where all of physical properties change.

Our hypothesis is that below 30 W of plasma power we observed real permeation, however above 30 W the films have defects – there are holes, and/or the films are formed from plates and active molecule can freely flow through these defects.

The permeation of CPB is shown in next figure (46)

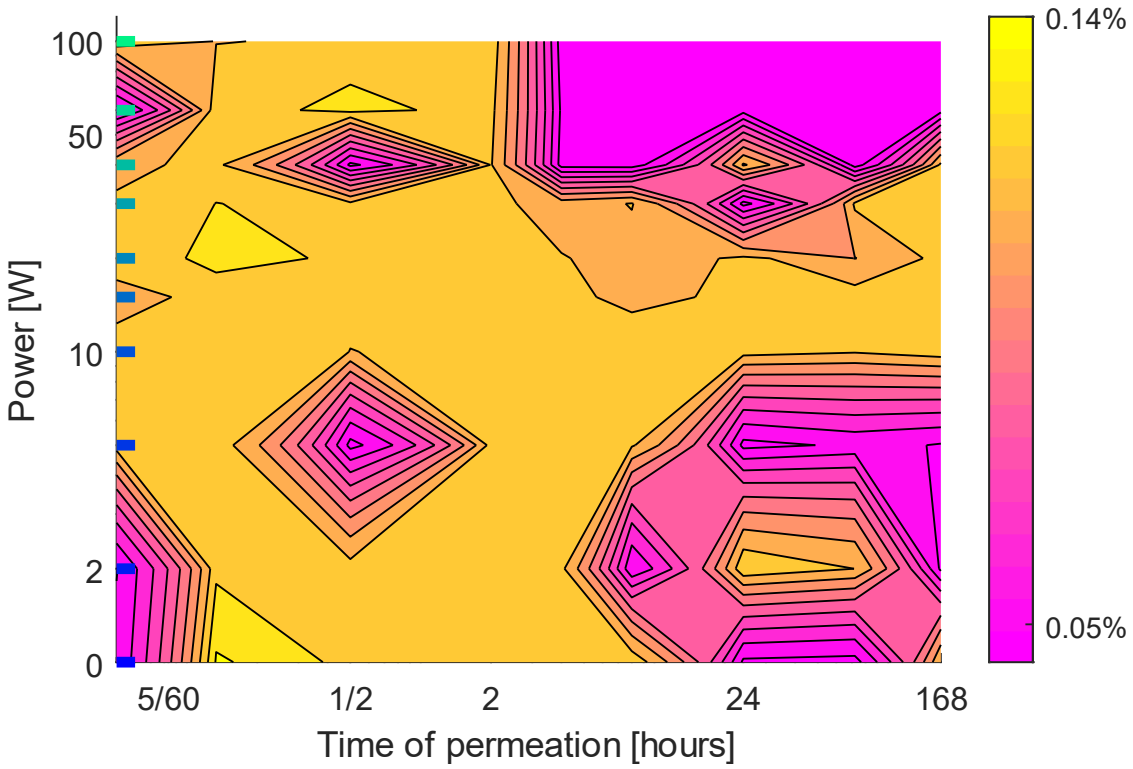

***Figure 49**. Graph of CPB permeation through the films The estimated concencration is shown with gradient of colour, where purple no CPB, yellow most CPB*

On the first observe no trend can be seen in results The CPB was observed at the samples taken at all times except the ones above 30W and below 10 W for long times. However, in the comparison with permeation through the Nisin similarities arise. In these regions above 30W and below 10 W in longer times Nisin also did not permeate. This basically means, that for lower powers the covering films was completely was off after two hours and there was no barrier layer, which protect the permeation. For the plasma power above 30 W same effect as for Nisin happened, where the CPB may went through the inhomogeneities. Therefore, it seems that the region, where CPB permeates is similar as for Nisin, but broader. This is in good agreement with the fact that the CPB is much smaller molecule.

3.4.7 Comparasion of Desolvation Hydrolisis and Permeation

To compare the time scales of previously mentioned properties of the films in water the figures (41), (44), (46), (47) are shown again in next figure (48). In the left column of the table are the miniatures of the figures (41), (44), (46), (47). In the right column the comparison with the thickness after/before immersion is depicted. To keep visualisation simple only the contours are shown. The contours in the graphs in the right column of thickness after/before immersion are shown with respect to original colour gradient. The compared property is depicted also in contours, but only in red colour.

	Compared property	Comparison with after/before immersion graph
After/before immersion	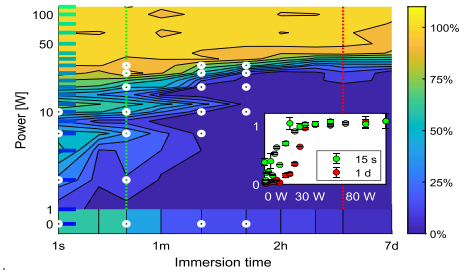	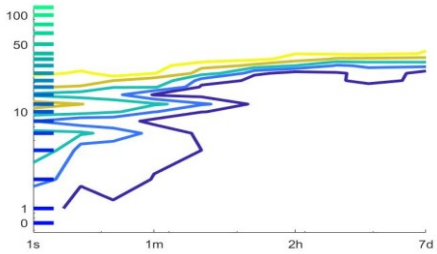
In-situ	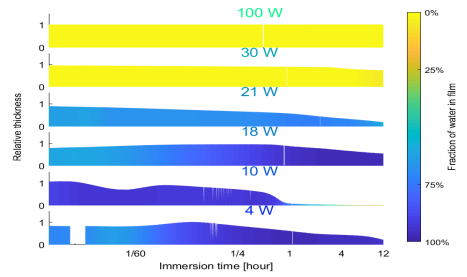	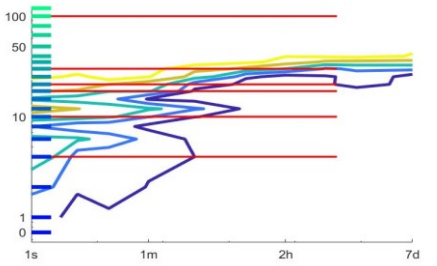
hydrolysis	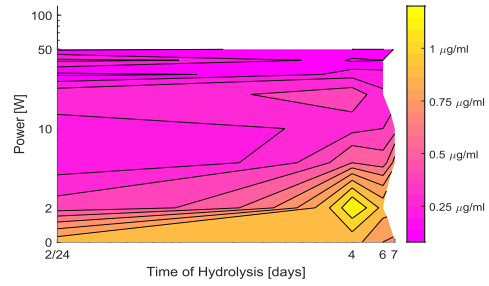	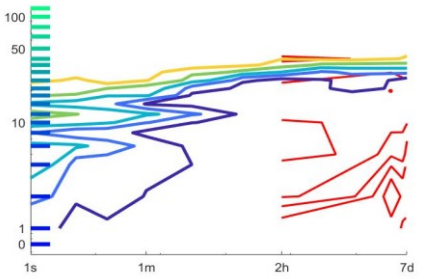
Nisin permeation	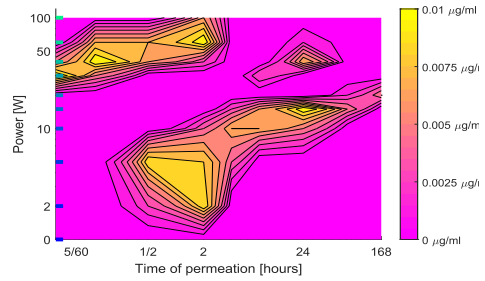	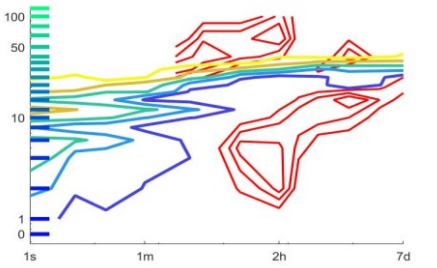
CPB permeation	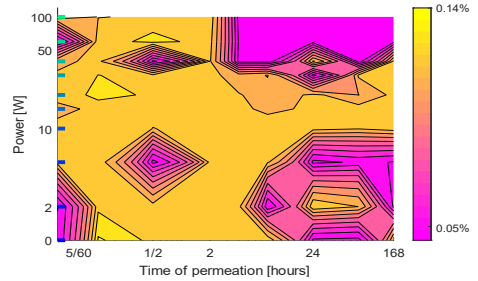	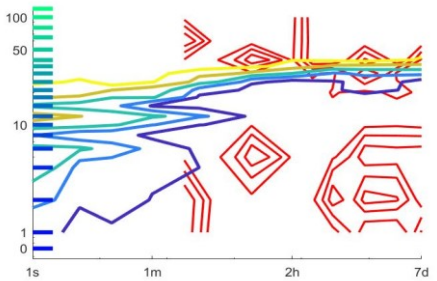

***Figure 50**. Summary graph of figures 41,44,46,48. The miniatures of these graphs are shown in left column. In the right column is comparison of graph 41 after/before*

immersion, where only contours are shown and respective graph 44(in-situ immersion),44(hydrolysis),47(Nisin),48(CPB), where only red contours are shown

As was mentioned in previous analysis the properties of the films can be divided into two regions - below 30 W of plasma power and above 30 W of plasma power.

Firstly, we discuss the region below 30 W of plasma power. As was mentioned in in-situ estimation of thickness the real time of dissolving is longer than the thickness after immersion predicts. The after/before immersion graph predicts that after ten minutes the film is washed off. However, in-situ measurements predict that the film still exists, but is swollen. The permeation through the films starts in a time scale of one hour. The swollen film is still present in this time scale. Therefore, this is a real permeation through the films. The permeation for lowest plasma powers (below 10 W) stops in time scale of two hours. This is in good agreement with in-situ results as almost all of the films are dissolved, as there is no film, which can protect the dissolution of the active molecules. For the films above 10 W and below 30 W of plasma power these properties are slower and end in time scale of several days. The process of hydrolysis starts in longer time scales than the permeation and only for samples prepared with lowest plasma powers. The film has to be completely dissolved to start hydrolysing.

Secondly, in the region above 30 W of plasma power different processes are important. The films are unsolvable in the whole time range where the measurements were done. However, the films do not protect the permeation process. The possible reason discussed in permeation chapter is, that the films have a defect or are formed by some plates. The hydrolysis did not occur for these films. The transition between weak hydrolysis and none hydrolysis can be found at 30 W of plasma power. This is in good agreement with the fact, that the films above 30 W of plasma power are unsolvable.

Conclusion

The aims of this thesis were successfully met as follows:

- The PAVTD setup was improved in terms of reproducibility and control of the deposition process.
- PLA-like films were prepared at a broad range of plasma power
- The composition of the films was characterised using combined information from XPS and NMR and approximate chemical structure of the plasma polymers was obtained. The resulting structure can be controlled from classical polymer-like to common plasma polymer.
- The films were characterised by their stability in water. Their swelling and hydrolysis properties cab be controlled. Their permeation properties for a set of model molecules were obtained

Bibliography

[1] A. Kausar, Survey on Langmuir–Blodgett Films of Polymer and Polymeric Composite, *Polym - Plast Technol Eng*, 2017, 56, 932–945, DOI: 10.1080/03602559.2016.1247282

[2] J. Y. Park, R. C. Advincula, Nanostructuring polymers, colloids, and nanomaterials at the air-water interface through Langmuir and Langmuir-Blodgett techniques. *Soft Matter,* 2011, 7, 9829–9843, DOI: 10.1039/c1sm05750b

[3] A. Fridman, *Plasma Chemistry*, Cambridge University Press, Cambridge, 2008

[4]H. Biederman, Introduction, *Plasma Polymer Films*, Imperial College Press, London, 2004

[5] [AI]M. Vaidulych*, Plasma Treatment of Porous Structures, Doctoral Thesis,* Charles University in Prague, Faculty of Mathematics and Physics, 2019

[6] H. Biederman, Y. Osada, *Plasma Polymerization Processes*, Elsevier, Amsterdam, 1992

[7] D. K. Lam, R. F. Baddour, A. F. Stancell, A Mechanisms and Kinetics Study of Polymeric Thin-Film Deposition in Glow Discharge, *J Macromol Sci Part A – Chem*, 1976, 10, 421–450, DOI: 10.1080/00222337608061191

[8] H. Biederman, Y. Osada, *Plasma Polymerization Processes*, Elsevier, Amsterdam, 1992

[8] P. Favia, Plasma deposition of fluoropolymer films in different glow discharge regimes, *Plasma Polymer Films*, Imperial College Press, London, 2004

[9] D. Hegemann, U. Schütz, E. Körner, Macroscopic Approach to Plasma Polymerization Using the Concept of Energy Density, *Plasma Processes and Polymers*, 2011, 8, 689-694, DOI: 10.1002/ppap.201000211

[10] B Nisol, S. Watson, S Lerouge, M.R. Wertheimer, Energetics of reactions in a dielectric barrier discharge with argon carrier gas: IV ethyl lactate, *Plasma process and polymers,*2016 ,13,10, 965-969 DOI:/10.1002/ppap.201600099

[11] A. Choukourov, J. Hanuš, J. Kousal, A. Grinevich, Y. Pihosh, D. Slavínská, H. Biederman, Thin polymer films from polyimide vacuum thermal degradation with and without a glow discharge, *Vacuum*, 2006, 80, 8, 923-929, DOI: 10.1016/j.vacuum.2005.12.012

[12] A. Choukourov, I. Melnichuk, I. Gordeev, O. Kylián, J. Hanuš, J. Kousal, P. Solař,

L. Hanyková, J. Brus, D. Slavínská, H. Biederman, Dynamic scaling and kinetic roughening of poly(ethylene) islands grown by vapor phase deposition, *Thin Solid Films*, 2014, 565, 249-260, DOI: 10.1016/j.tsf.2014.06.029

[13] A. Choukourov, I. Gordeev, D. Arzhakov, A. Artemenko, O. Kylián, J. Kousal, O. Polonskyi, J. Pešička, D. Slavínská, H. Biederman, Nanocomposite gold/poly(ethylene oxide)-like plasma polymers prepared by plasma-assisted vacuum evaporation and magnetron sputtering, *Surface and Coatings Technology*, 2011, 205, 8-9, 2830-2837, DOI: 10.1016/j.surfcoat.2010.10.055

[14] A. Choukourov, I. Gordeev, D. Arzhakov, A. Artemenko, J. Kousal, O. Kylián, D. Slavínská, H. Biederman, Does Cross-Link Density of PEO-Like Plasma Polymers Influence their Resistance to Adsorption of Fibrinogen? *Plasma Process. Polym.* 2012, 9, 48–58, DOI: 10.1002/ppap.201100122

[15]. Choukourov, A. Grinevich, O. Polonskyi, J. Hanus, J. Kousal, D. Slavinska, H. Biederman, Vacuum Thermal Degradation of Poly(ethylene oxide), *J. Phys. Chem. B*, 2009, 113, 10, 2984-2989, DOI: https://doi.org/10.1021/jp8107107

[16] P. P. Luff, M. White, The structure and properties of evaporated polyethylene thin films, *Thin Solid Films*, 1970, 6, 3, 175-195, DOI: 10.1016/0040-6090(70)90038-6

[17] P. P. Luff, M. White, Thermal degradation of polyethylene and polytetrafluoroethylene during vacuum evaporation, Vacuum, 1968, 18, 8, 437-440, DOI: 10.1016/0042-207X(68)90336-9

[18] A. J. Domb, J. Kost, D. M. Wiseman, *Handbook of Biodegradable Polymers*, CRC Press, Boca Raton, 1997.

[19] A. Lendlein, A. Sisson, *Handbook of Biodegradable Polymers: Isolation, Synthesis, Characterization and Applications*, John Wiley & Sons, Weinheim, 2011.

[20] I. Vroman, L. Tighzert, Biodegradable Polymers, *Materials*, 2009, 2 307-344, DOI:10.3390/ma2020307

[21] C. S. Ha, Jr J. Gardella, Surface Chemistry of Biodegradable Polymers for Drug Delivery Systems, *Chemical Reviews*, 2015, 105, 4205–4232, DOI: 10.1021/cr040419y

[22] H. Zhou, J. G. Lawrenc, S. B. Bhaduri, Fabrication aspects of PLA-CaP/PLGA-CaP composites for orthopedic applications: a review, *Acta Biomaterialia*, 2012, 8, 1999-2016, DOI: 10.1016/j.actbio.2012.01.031

[23] P. Kucharczyk, E. Hnátková, Z. Dvořák, V. Sedlařík, Novel aspects of the

degradation process of PLA based bulky samples under conditions of high partial pressure of water vapour, *Polymer Degradation and Stability*, 2013, 98, 150-157, DOI: 10.1016/j.polymdegradstab.2016.04.019

[24] H. Tian, Z. Tang, X. Zhuang, X. Chen, X. Jing, Biodegradable synthetic polymers: Preparation, functionalization and biomedical application, *Progress in Polymer Science*, 2012, 37, 237-280, DOI: 10.1016/j.progpolymsci.2011.06.004

[25] M. Oliveira, E. Santos, A. Araujo, G. M. J. Fechine, A. V. Machado, G. Botelho, The role of shear and stabilizer on PLA degradation, *Polymer Testing*, 2016, 51, 109-116, DOI: 10.1016/j.polymertesting.2016.03.005

[26] A. E. Swilem, M. Lehocký, P. Humpolíček, Z. Kučeková, I. Novák, M. Micušík, H.A. Abdel-rehim, E. A. Hegazy, A. A. Hamed, J. Kousal, Description of D-glucosamine immobilization kinetics onto poly(lactic acid) surface via a multistep physicochemical approach for preparation of novel active biomaterials, *Journal of Biomedical Materials Research: Part A*, 2017, 105A, 3176-3188, DOI: 10.1002/jbm.a.36158

[27] Y.-B. Luo, W.-D. Li, X.-L.Wang, D.-Y. Xu, Y.-Z. Wang, Preparation and properties of nanocomposites based on poly(lactic acid) and functionalized TiO2, Acta Materialia, 2009, 57,3182–3191. DOI:10.1016/j.actamat.2009.03.022

[28] P. Kucharczyk, E. Hnatkova, Z. Dvorak, V. Sedlarik, Novel aspects of the degradation process of PLA based bulky samples under conditions of high partial pressure of water vapour, *Polymer Degradation and Stability 2013*, 98, 150-157. DOI:10.1016/j.polymdegradstab.2016.04.019

[29] D. Nikitin, Structuring of plasma polymers: new methods for fabrication of nano-architectured thin films, Doctoral Thesis, Charles University in Prague, Faculty of Mathematics and Physics, 2019

[30]J. Kousal, **Z. Krtouš**, Z. Kolářová Rašková, J. Sedlaříková, J. Schäfer, L. Kučerová, A. Shelemin, P. Solař, A. Hurajová, H. Biederman, M. Lehocký, Degradable plasma polymer films with tailored hydrolysis behavior, *Vacuum*, 2020, 173, 109062, DOI: 10.1016/j.vacuum.2019.109062

[31]K. Yuniarto, Y. A. Purwanto, S. Purwanto, B. A. Welt, H. K. Purwadaria, T. C. Sunarti, *Infrared and Raman studies on polylactide acid and polyethylene glycol-400 blend,* AIP Conference Proceedings, 2016, 1725, 020101, DOI: 10.1063/1.4945555

[32]J. F. Moulder, W. F. Stickle, P. E. Sobol, K. D. Bomben, *Handbook of X-ray*

Photoelectron Spectroscopy, Minnesota, 1995

[33]J. Kousal, *Diagnostika procesu plazmové polymerace, Doktorská disertační práce*, Univerzita Karlova v Praze, Matematicko-fyzikální fakulta, 2006

[34]V. Cech, R. Trivedi, D. Skoda, Mechanical Properties of Individual Layers in a-SiC:H Multilayer Film, *Plasma Process. Polym.* 2011, 8, 1107-1115, DOI: 10.1002/ppap.201100106

List of Tables

List of Figures

Figure 18. The measured XPS spectra. The colour gradient distinguish between samples varying in the power of plasma used for preparation. O1s part rescaled by relative sensitivity factor. The overall area of C1s and O1s is renormalized on 1 for all plasma powers.

Figure 19. The comparison between measured XPS data (blue-green colour gradient depicts plasma power used for preparation sample) and fit (black-bronze colour gradient) with just PLA structure. The difference between fit and measured data is shown below the comparison with offset. The actual fit decomposition can be found on figure 20.

Figure 20. The decomposition of fit with just PLA structure. Black-bronze colour gradient distinguish plasma power used for preparation. The dashed lines are the envelope curves on fit. The C1, C2.1, C3, O1, O2.1 are tabulated energetic position of PLA peaks

Figure 21. Chemical composition according to XPS (fitted with just PLA peaks) in dependence on plasma power used for preparation of samples The C1, C2.1, C3, O1, O2.1 corresponds to tabulated PLA peaks

Figure 22. The XPS model consisting just PLA structure do not correctly assign the C-O-C structures. a) model b) hypothetical structure

Figure 23. The decomposition of fit with fitted energy position of C2.x peak. Black-bronze colour gradient distinguish plasma power used for preparation. The dashed lines are the envelope curves on fit. The C1, C2.1, C3, O1, O2.1 are tabulated binding energy of PLA peaks and C2.2 is tabulated peak of PEG

Figure 24. The comparison between measured XPS data (blue-green colour gradient depicts plasma power used for preparation sample) and fit (black-bronze colour gradient) with PLA and ether structure. The difference between fit and measured data is shown below the comparison with offset. The actual fit decomposition can be found on figure 25.

Figure 25. The decomposition of fit with PLA and ether structure. Black-bronze colour gradient distinguish plasma power used for preparation. The dashed lines are the envelope curves on fit. The C1, C2.1, C3, O1, O2.1 are tabulated binding energy of PLA peaks, C2.2 and O2.2 are PEG peaks

Figure 26. Chemical composition according to XPS (fitted with PLA and ether structure) in dependence on plasma power used for preparation of samples The C1, C2.1, C3, O1, O2.1 corresponds to tabulated PLA peaks

Figure 45. In-situ swelling of the films measured by ellipsometry with samples in liquid cell. The thickness in time is depicted on the y axis of the graphs, the amount of water is depicted as colour gradient. Dark blue corresponds to water, yellow to solid film.

Figure 46. Hydrolysis reaction of PLA

Figure 47. Graph of hydrolysis. The estimated concentration is shown with gradient of colour, where purple no LA, yellow most LA

Figure 48. Graph of Nisin permeation through the films. The estimated concentration is shown with gradient of colour, where purple no Nisin, yellow most Nisin

Figure 49. Graph of CPB permeation through the films. The estimated concentration is shown with gradient of colour, where purple no CPB, yellow most CPB

Figure 50. Summary graph of figures 41,44,46,48. The miniatures of these graphs are shown in left column. In the right column is comparison of graph 41 after/before immersion, where only contours are shown and respective graph 44(in-situ immersion),44(hydrolysis),47(Nisin),48(CPB), where only red contours are shown

Abbreviations

BSA	bovine serum albumin
CPB	cetyl pyridinium bromide
CVD	chemical vapor deposition
DBD	dielectric barrier discharge
DEPT	distortionless enhancement by polarization transfer
eV	electron volt
FTIR	Fourier transformer infrared spectroscopy
FWHM	full width at half maximum
GPC	gel permeation chromatography
HMQC	multiple quantum coherence
N	nisin
NMR	nuclear magnetic resonance
PAVDT	plasma assisted vapour thermal deposition
PECVD	plasma enhanced chemical vapour deposition
PLA-PEG	poly lactic acid poly ethylene glycol
PLA	poly lactic acid
PVD	physical vapor deposition
QCM	quartz crystal microbalance
RF	radio frequency
SEM	scanning electron microscopy
SS	sodium salicylate
WCA	water contact angle
XPS	X-ray photoelectron spectroscopy

List of Publications

Reviewed international journals

1. P. Pleskunov, D. Nikitin, R. Tafiichuk, A. Shelemin, J. Hanuš, J. Kousal, **Z. Krtouš**, I. Khalakhan, P. Kuš, T. Nasu, T. Nagahama, C. Funaki , H. Sato, M. Gawek, A. Schoenhals, A. Choukourov, Plasma polymerization of acrylic acid for tunable synthesis of glassy and carboxylated nanoparticles, *ACS J. Phys. Chem.* (in review process)
2. J. Kousal, **Z. Krtouš**, Z. Kolářová Rašková, J. Sedlaříková, J. Schäfer, L. Kučerová, A. Shelemin, P. Solař, A. Hurajová, H. Biederman, M. Lehocký, Degradable plasma polymer films with tailored hydrolysis behavior, *Vacuum*, 2020, 173, 109062, DOI: 10.1016/j.vacuum.2019.109062
3. J. Kousal, A. Shelemin, M. Schwartzkopf, O. Polonskyi, J. Hanuš, P. Solař, M. Vaidulych, D. Nikitin, P. Pleskunov, **Z. Krtouš**, T. Strunskus, F. Faupel, S. Roth, H. Biederman, A. Shoukorov, Magnetron-sputtered copper nanoparticles: lost in gas aggregation and found by in situ X-ray scattering, *Nanoscale,* 2018, 10, 18275-18281

Conference proceedings

1. L. Kučerová, Z. Kolářová Rašková, J. Kousal, **Z. Krtouš**, P. Solař, J. Sedlaříková, M. Lehocký, Polyester urethane (PLA/PEG) polymer based films prepared by plasma assisted vapour thermal deposition, *NANOCON 2019 - Conference Proceedings* (in review process)
2. **Z. Krtouš**, A. Nikiforov, I. Kuchakova, Z. Kolářová Rašková, J. Sedlaříková, T. Kretková, P. Kuš, O. Kylián, J. Kousal, Nanostructured Films of plasma polymerized hexamethyldisilazane and lactic acid deposited by atmospheric plasma jet, *NANOCON 2019 - Conference Proceedings* (in review process)
3. J. Kousal, Z. Kolářová Rašková, J. Sedlaříková, P. Stloukal, P. Solař, **Z. Krtouš**, A. Choukourov, V. Sedlařík, Plasma polymers with controlled degradation behaviour, *NANOCON 2017 - Conference Proceedings*, 2018, 461 – 466
4. S. Ali-Ogly, L. Kučerová, **Z. Krtouš**, and J. Kousal, Surface Modification by Plasma-Based and Related Methods Demonstrated on Magnetron Sputtering of Polylactic Acid, *WDS 2019 Conference Proceedings* (in review process)

Conference contributions presented by author

1. NANOCON 2019 – Brno, Czech Republic: Nanostructured films of plasma polymerized hexamethyldisilazane and lactic acid deposited by atmospheric plasma jet (poster)
2. Nanoworkshop 2019 – Helsinki, Finland: Plasma polymer films prepared using plasma-assisted vapour thermal deposition of PLA (poster)
3. COPSA 2018 – Ieper, Belgium: Characterization of control of properties of thin films prepared using plasma-assisted vapour thermal deposition from biodegradable precursors (oral presentation)
4. SPPT 2018 – Prague, Czech Republic: Properties of plasma polymer films based on classical polymers (poster)
5. JVC 2018 – Olomouc, Czech Republic: Semi-analytical model of thermal coalescence of nanoparticles (poster)
6. Nanoworkshop 2017 – Prague, Czech Republic: Temperature changes in thin films of nanoparticles